Universidad de Guanajuato
División de Ciencias Naturales y Exactas

Revisiting the Wilson-Bappu Effect

Por

Cecilia María Guerra Olvera

Una tesis sometida al

Departamento de Astronomía

como requisito para la obtención del grado de

MAESTRÍA EN CIENCIAS

Astrofísica

Aprobada por:

Dennis Jack, Supervisor de Tesis

K.-P. Schröder, Supervisor de Tesis

Gto., Guanajuato
Junio, 2014.

Abstract

I use the versatile PHOENIX atmosphere modeling code, which includes a gravity scaled chromosphere above the temperature minimum to model the Ca II K emission line profile for solar type stars, all with T_{eff} =5,780 K and same turbulence broadening, only with different surface gravities. Models, which produce the modest emission observed in relatively inactive stars, reproduce the Wilson-Bappu effect (WBE) in absolute terms, i.e. the emission line-widths grow with lower gravity consistent with $W_0 \propto g^{-0.17}$ in the range of $\log(g) = 5.0$ to 3.5.

In the solar case, which was used as a first test, I find the temperature minimum (over height, single component) for a relatively inactive Sun to reach down to 3,930 K. The respective PHOENIX model ($\log(g) = 4.4$) matches width and typical flux of the chromospheric Ca II emission of a nearly inactive Sun, as observed with the Hamburg Robotic Telescope, and also matches the solar W_0 of 0.44 Å. For comparison, the quiet Sun model (figure 1.3) of Vernazza et al. (1973) had a temperature minimum of 4,170 K.

Using the solar effective temperature, I then computed models with different gravity in order to see if these would reproduce the WBE. A practical problem occurs in that the shallow basal flux emission is too smeared out at already $\log(g) = 3.5$. Consequently, I needed to make the bottom of the chromosphere (just above the temperature minimum) a little warmer to mimic the emission of modestly active stars, which in fact represent the stars observed for the WBE. But the equilibrium conditions allow only for a small margin on this.

I do not adjust any other parameter than surface gravity to obtain the emission line profiles. Hence, these are produced from first principles and so represent a good test of the WBE explanation given by Ayres et al. (1975), 40 years ago. As a result, the line widths reproduce the observed WBE gravity dependence with an exponent of -0.17 (rather than -0.25) very well and in absolute terms.

Contents

Acronyms

AGN	Active Galactic Nuclei
EOS	Equation of State
HRD	Hertzsprung-Russell Diagram
LTE	Local Termodynamic Equilibrium
MPI	Message Passing Interface
MSS	Main-Sequence Star
NLTE	Non-local Termodynamic Equilibrium
OSI	Operator Splitting Iteration
QDA	Quad-Double Arithmetic
RTE	Radiative Transfer Equation
TR	Transition Region
WBR	Wilson-Bappu Relation

List of figures and tables

1 Introduction

1.1. Motivation

The *Wilson-Bappu effect* describes the observed increase of the width of the chromospheric Ca II (as well as Mg II) emission lines of cool stars and giants with increasing luminosity and hence, decreasing gravity. This is a well-defined relation, which hardly depends on any other parameters, and that can be derived from inactive or active stars.

Despite the WB effect was discovered 57 years ago, and it has been understood in principle since 40 years, it has still not been modeled precisely because (1) chromospheric models are in general not trivial and require a good photospheric model to start with, and (2) the easier to observe emission of active stars is known to not follow the WB effect reliably.

The stellar and planetary atmosphere code package PHOENIX has been developed and steadily improved over two decades. It can calculate atmospheres all across the HR-diagram as well as rapidly expanding atmospheres as found in novae and supernovae. The PHOENIX code comes with a very rich opacity library (including molecules), and a state-of-the-art equation of state, hence, it is capable of handling very cool temperatures as those found in giant stars.

In addition, the PHOENIX code manages atmospheres in spherical geometry and also accounts for extreme NLTE conditions, which are both important issues for modeling chromospheres of giants. Furthermore, this code already has a mode to include a chromosphere in a semi-empirical way in the stellar spectra. This chromospheric mode has been successfully applied by modeling M-dwarf chromospheres.

Well-tested, accurate photospheric PHOENIX models already exist for cool giants, but these artificially end in the temperature minimum. Hence, all weak and medium photospheric lines are matched excellently. But emission from the chromospheres, as observed in the very strongest lines such as Ca II K, caused by the outwardly increasing tempera-

ture in the chromospheric layers, has so far been left unconsidered.

The fundamental nature of this problem and since no quantitative chromospheric models exist so far, make the Wilson-Bappu effect a problem that has fascinating the experts in the field since it was first discovered. In addition, it has neither been reproduced to fully match the observational evidence.

Today's much improved knowledge of stellar activity, accurate distances and computational power allow us to revise and improve the observed Wilson-Bappu effect and to finally use it as a principal guide and benchmark-test for models of the inactive chromosphere, which is governed by relatively simple equilibrium physics.

This work aims on reproducing a very modest emission of stars with different gravities not much above the basal flux by using the chromospheric extension of the PHOENIX code.

1.2. Stellar atmospheres

If we imagine a star as a family of spherical layers of different radii sorted one next to another, we can study it by regions formed by a certain number of these layers. Of course this is only a simplification, and although we study stars by regions, all of them are interacting with each other and cannot be completely physically detached. Following this scheme, from the core outward are the radiative zone, the convection zone, the photosphere, the chromosphere, a transition region, and a corona (figure 1.1). The atmosphere is the region surrounding a star and it goes from the photosphere through the corona.

This region is of great importance because it is a transition region between the interior of a star and the interstellar medium. At the same time, the atmosphere is subdivided into smaller sections which are a function of kinetic temperature[1]: sub-photosphere, photosphere, chromosphere, transition region, and corona.

The radiation transmitted into space from a star, which is the one we see and measure, is emitted from the photosphere. This is the region where deep layers (towards the core) of a star start to be visible, i.e., it is the outermost opaque layer but its opacity (τ) is smaller than 1. The radiation emitted in deeper zones than the photosphere will not escape and will not reach us because the high temperatures and densities do not allow the material within it to leave, and material in the outer zones having low density and $\tau \ll 1$ will hardly emit radiation.

[1]Temperature of atoms due to their random velocities.

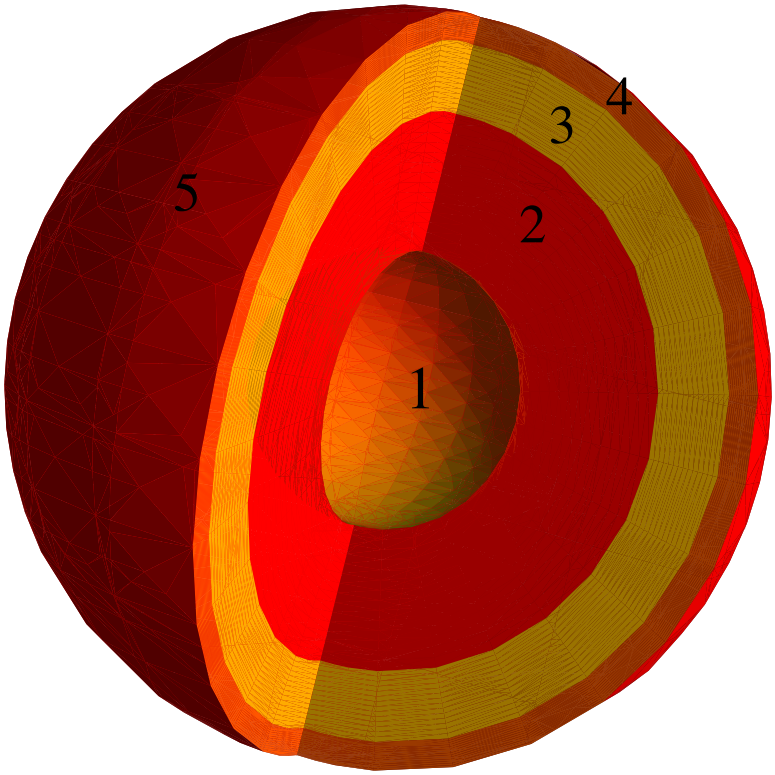

Figure 1.1.: Scheme of solar interior structure. The zones are labeled as follows: 1) Stellar core, 2) Radiative zone, 3) Convective zone, 4)Photosphere, and 5) Chromosphere. The corona is the region surrounding the chromosphere, and the transition region is located between them. The scheme is not scaled.

The temperature drops across the photosphere until a minimum temperature value is reached, which is the beginning of the chromosphere. After that point, temperatures will rapidly increase with height (h). The photosphere's height or thickness varies for different kinds of stars as $h \propto g^{-1}$, where g is the surface gravity. For the Sun this value is of about 1,000 kilometers and its density is around $10^{-8} g/cm^3$.

Although the stellar radiation we receive comes from photospheres, the energy itself is produce in deeper zones of the stellar interior, where nuclear reactions take place. For the energy to reach the optically thin region, it has to be transported to outer zones by means of convection or radiation. But convection is not always possible, its viability is determined by the *Schwarzschild criterion*[2] which establishes that the radiative temperature gradient has to be smaller than the adiabatic temperature gradient to assure convection:

$$\left|\frac{dT}{dr}\right|_{ad} < \left|\frac{dT}{dr}\right|_{rad} \tag{1.1}$$

[2]Proposed by K. Schwarzschild in 1906.

Furthermore, convection does not always occur at central zones but can be present in the outer zones as well. For hot stars ($T \sim 10,000$ K), central convection is seen due to the high luminosities produced at their cores, while for cool stars like the Sun (T_{eff} =5,780 K) convection is more likely to be present at outer zones.

When the density gradient ($\frac{1}{\rho}\frac{d\rho}{dr}$) is much more steeper than the temperature gradient ($\frac{1}{T}\frac{dT}{dr}$), we can write

$$\frac{1}{\rho}\frac{d\rho}{dr} \gg \frac{1}{T}\frac{dT}{dr} \tag{1.2}$$

But increasing density will have a direct effect on the gas pressure (P_{gas}), and the same goes for the temperature gradient with radiation pressure (P_{rad}). Hence, equation (1.2) can be rewritten as

$$P_{gas} \gg P_{rad} \tag{1.3}$$

On the other hand, if we assume to have an ideal gas in the atmosphere, the internal energy of such gas will be in the form of kinetic energy. In addition, any change in internal energy will be accompanied by a change in temperature. Following this assumption, the ideal gas law tells us that

$$\begin{aligned} PV &= nRT \\ \rightarrow P &= \frac{nRT}{V} \\ \rightarrow P &= \frac{m}{M}\frac{RT}{V} \\ \rightarrow P &= \frac{\rho RT}{M} \end{aligned} \tag{1.4}$$

where n is the molar number, m is the mass of the gas, M its molar mass, V the volume it occupies, T the temperature and R the gas constant. Equation (1.4) is particularly interesting because it links the three more important parameters of gases (ρTP).

In statistical mechanics, while working with particles, the gas constant is equivalent to $R = N_A\kappa$, with κ and N_A being the Boltzmann and Avogadro constant, respectively. The latter can also be represented as $N_A = M/m_u$, where M is the molar mass constant and m_u is the atomic mass unit. Hence, for a particle of mass μ times the atomic mass, equation (1.4) is

$$P = \kappa T\rho\frac{1}{\mu m_u} \tag{1.5}$$

where $\rho = nM/V$ is the mass density of the particle. Furthermore, from hydrostatic equilibrium we know that $\frac{dP}{dr} = -\rho(r)g$, feeding (1.5) into this:

$$\begin{aligned} &\frac{d}{dr}\left[\kappa T\rho\frac{1}{\mu m_u}\right] = -\rho(r)g \\ &\rightarrow \kappa T\rho\frac{1}{\mu m_u}\frac{d\rho}{dr} = -\rho(r)g \\ &\rightarrow \frac{d\rho}{dr} = -g\mu m_u\frac{1}{\kappa T}\rho(r) \end{aligned} \tag{1.6}$$

The solution to (1.6) is an exponential function modulated by the initial value $\rho_0 = \rho(r_0)$, where the scale height is defined as $h_0 = \frac{g\mu m_u}{\kappa T}$ and $h = r - r_0$. This equation is shown below, and it is known as the *Barometric Law*.

$$\rho(r) = \rho_0 e^{h/h_0} \tag{1.7}$$

The Barometric Law tells us that for each distance h_0, density will change by a factor of e. In giant stars, which have big scale heights, one find very low densities if compared with MSS. The solar scale height is about $h_0 \sim 300\ km$.

1.3. Model atmosphere

Analyzing stellar spectra provides the opportunity to study stars and to get a great amount of information about the physical state of their atmospheres. Although energy production takes place in the core of stars, all the radiation we measure has to first pass through an atmosphere. This process will throw light on the factors not only of the core but of the entire atmosphere as well.

Some examples of stellar parameters determined from spectra are radial velocity, which is gotten by measuring the shifted lines due to the Doppler effect, effective temperature[3] by observing certain absorption lines that are representative of temperature ranges because their atomic transitions can only exist at such energy extend or by finding the maximum intensity to apply Wien's law (see figure 1.2), and chemical composition, between others.

[3]Temperature of a black body having the same luminosity and radius as the star.

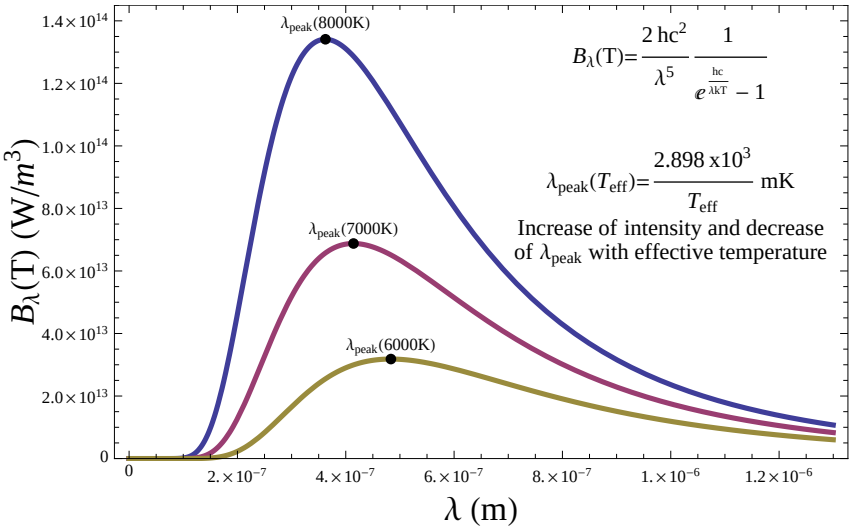

Figure 1.2.: Scheme of Wien's law. The curves represent Planck's functions for the different indicated effective temperatures, while the black dots indicate the respective wavelengths at which the emission has its maximum.

All of the above measurements require thorough analysis, and a meticulous interpretation cannot be made in some cases. It is then when we are encouraged to make physical assumptions and create hypothesis trying to reproduce and, even more important, to explain the features concerning the incoming radiation. Such hypothesis are turned into a model which must obey physical laws and match observations that will be basically used to test it. If needed, the model is modified to bear accurate resemblance to the available observations and once that has been done, one can think in using it to reproduce phenomena. Furthermore, when a model is worth of trust, it may also be used to understand properties of stars that in other cases would remain as an enigma. It has to be established then, that theoretical models are elemental in modern astrophysics.

In the case of model photospheres, one often refers to a "classical model atmosphere" where only the photosphere is being calculated and not the chromosphere, transition region, nor stellar winds. However with the increase of research in the field, the development of new and modern codes, and the increasing computer power, nowadays it is hard to label one model as the classical one. Nonetheless, the most common way to produce such models is to assume energy conservation, hydrostatic equilibrium, LTE, and plane parallel geometry or spherical symmetry for geometrically extended stars.

How valid and reliable these assumptions are will depend on the desired degree of detail we are working with, and on many more physical properties that can be included without producing an inconsistent model. A clear example of the latter is the so-called line blanketing, which causes models to give the impression of being blue shifted with respect to observations, specially for cool stars where the red/infrared part of the spectrum appears

enhanced relative to a star with a non-blanketed spectrum.

On the other hand, since the line formation problem consists in solving two equations simultaneously, it is one of the biggest challenges when modeling photospheres. In order to get through this, it is necessary to apply numerical methods that allow us to solve (1) the radiative transfer equation for all the wavelengths we are interested in and (2) the equation of statistical equilibrium when NLTE is used, i.e., the line source function; the analogous for LTE is the Boltzmann equation (A.6). The implementation of Accelerated Lambda Iteration (ALI) methods, well described by Hubeny (2003), is very popular in stellar atmosphere modeling to obtain a formal solution of such problem due to the high degree of complexity and accuracy it offers.

1.4. Chromospheres

A stellar chromosphere is a region within the atmosphere of a star where the temperature increases outwards after a minimum temperature value (T_{min}) is reached in the upper part of the photosphere and it is found in cool late type stars of spectral type F, G, K, and M. This effect is known as temperature reversal and can be detected through spectral analysis, specially in lines whose optical depth is high in the chromosphere and whose behavior within it differs from that within the photosphere (Zirin, 1971). Carrying on this spectral analysis one would be able to tell wether a line has been formed in the chromosphere and hence prove the existence of a temperature reversal. The region in the atmosphere where this effect is seen is also known as *reversing layer*.

A value of about 4,300 K for the temperature minimum for the Sun was proposed by Avrett and Linsky (1970), who solved the hydrostatic and ionization equilibrium equations to produce a solar atmospheric model; they also found the chromosphere's properties to be relevant in the shaping of the wings of singly ionized calcium (Ca II). In a similar way and although some large error bars on observations, the *Harvard Smithsonian Reference Atmosphere* (Gingerich et al., 1971) predicts a 4,170 K minimum; such model is consistent with observational data on different wavelengths including ultraviolet, visible and infrared spectrum.

But probably the most famous chromosphere model is that of Vernazza et al. (1973), who determined an empirical temperature distribution for the solar atmosphere, the "so-called" VAL models. They adopted a slightly smaller value for the temperature minimum than the previous models, setting it to 4,000±100 K in order to have a spectrum that agrees with solar observations between 505 Å and 1.5 cm.

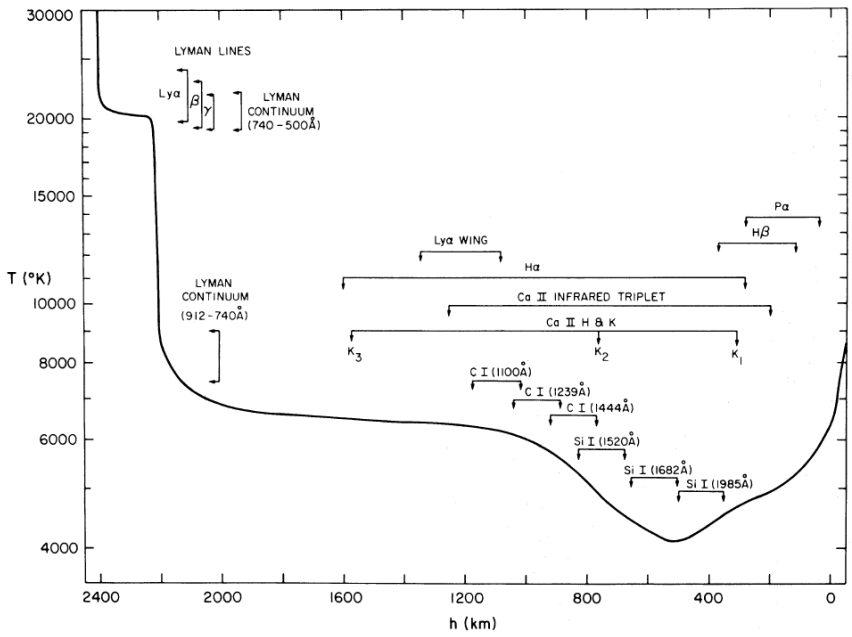

Figure 1.3.: Solar atmosphere temperature-height distribution as determined by Vernazza et al. (1973). Height is given in kilometers measured above zero point where $\tau = 1$. Regions of line formation are also indicated. From right to left: photosphere, temperature minimum (4,100 K), chromosphere, transition region ($> 8,500$ K), Lyman valley (20,000 K), and corona.

This model was obtained by trial-and-error temperature adjustments and it includes some arbitrary values in regions where spectra provided little information about the temperature structure (region between 1,000 and 2,200 km in figure 1.3), as well as a relatively low temperature maximum in the chromosphere of 8,500 K. Despite these assumptions, this model is by far the most accepted and cited model atmosphere to date.

1.4.1. Physics of chromospheres

As we saw in the previous section, the dependence of h_0 on g it is mainly determined by the properties of the particles within the photosphere. But when we move outwards through the chromosphere, gravity will play an important role in the way density changes and the consequences of it.

In the chromosphere, low density values turn out into lower collision rates that can be compared with radiative rates. In this case, pressure is mostly caused by turbulent motions and can be calculated from the kinetic energy (E_K) that produces such motions:

$$\begin{aligned} E_K &= \frac{1}{2}mv^2 \\ \rightarrow E_K &= \frac{1}{2}(\rho V)v^2 \\ \rightarrow P &= \frac{1}{2}v^2\rho \end{aligned} \tag{1.8}$$

where $P = \frac{E_K}{V}$, v is the turbulent velocity, m the mass of the particles and V the volume they occupy. Assuming hydrostatic equilibrium $\left(\frac{dP}{dr} = -\rho(r)g\right)$ we get

$$\frac{d\rho}{dr} = -\frac{2g}{v^2}\rho \tag{1.9}$$

whose solution is given by

$$\rho(r) = \rho_0 e^{-\frac{2g}{v^2}h} \tag{1.10}$$

Hence, scale heights for chromospheres $\left(h_0 = \frac{v^2}{2g}\right)$ go up with lower gravity and densities become smaller.

But what makes the presence of a chromosphere possible? First of all, a temperature reversal indicates that atmospheres holding chromospheres are not in radiative equilibrium as thought before, i.e., temperatures do not diminish radially through the atmosphere, and a responsible physical mechanism for this reversal has not yet been fully determined, but well studied. However, the more relevant processes for chromospheric heating have been determined to be magnetic heating by magnetic field dissipation and acoustic waves by shock dissipation, alone or both together (Narain and Ulmschneider, 1990; Ulmschneider, 2003; Kraft et al., 1964). Chromospheres lose large amounts of energy by radiation, hence their heating mechanism has to be effective enough to prevent them from cooling.

Heating by dissipation of acoustical waves has been extensively supported in the literature since the discovered of such high temperatures in the atmospheres. Acoustic waves are supposed to be generated by convective motions in the upper zones of the photosphere. These waves propagate naturally in an outward direction and carry certain amount of energy that depends on their velocity (v) and density (ρ) (Narain and Ulmschneider, 1990):

$$F = v^2 \rho c_s \tag{1.11}$$

where F is the mechanical energy flux and c_s the sound speed. As the outer zones of the atmosphere have smaller densities, the waves' amplitude will increase, which can also be translated as an increment of transported energy, forming shocks and heating the surrounding medium.

The most significant way in which magnetic fields promote the heating of chromospheres is by direct dissipation forced by large scale magnetic flows. The idea is that when they encounter smaller magnetic zones (like sunspots) sufficiently close to produce an effect on them, the fields immersed in these regions will be shrunk together causing dissipation of magnetic energy (Ulmschneider, 2003).

Activity is also used to study the properties of phenomena within the chromosphere. The most important parameter for measuring activity is without doubt the *Mount Wilson S-index*, whose measurements began with the *Mount Wilson HK-Project* in 1966 (Wilson, 1978). The S-index was defined with a four-channel spectrophotometer that was built specially for the measurement of stellar chromospheric calcium emission (Vaughan et al., 1978). It is a composition of these channels as follows:

$$S = \alpha \frac{N_H + N_K}{N_V + N_R} \tag{1.12}$$

where N_H, N_K, N_V, and N_R are the photon counts in the H and K line cores, in 4001.07 Å, and in 3901.07 Å, respectively. Moreover, the S-index has been used to calculate activity periods, to classify variable and ciclic stars (Baliunas et al., 1995).

So far we have seen some aspects of the chromosphere that are very important to construct such a structure and to understand the basics of its behavior. But how does the physics of the photosphere differs from that of the chromosphere?. There are a few things which have to be treated in a different way between them because, since the physical conditions are different, we cannot just apply the same rules neither expect the same laws to define the environment. Those aspects are to be listed in table 1.1.

Photosphere	**Lower chromosphere**	**Upper chromosphere**
High density values ($\sim 10^{-7} gr/cm^3$)	Low density values ($\sim 10^{-11} gr/cm^3$)	Extremely low density values ($\sim 10^{-14} gr/cm^3$)
Collisional rate $\gg$ Radiative rates	Collisional rate $\sim$ Radiative rates	Collisional rate $\ll$ Radiative rates
C_{21},C_{12} $\gg$$B_{12}$,$B_{21}$	C_{21},C_{12} $\sim$$B_{12}$,$B_{21}$	C_{21},C_{12} $\ll$$B_{12}$,$B_{21}$
LTE: $T_{e^-} = T_{exc} = T_{ion} = T_{rad}$	Near LTE: $T_{e^-} \sim T_{exc} \sim T_{ion} \neq T_{rad}$	non-LTE: $T_{e^-} \neq$ other temperatures
$S_\nu = B_\nu(T)$	$S_\nu = \epsilon B_\nu(T) + (\epsilon - 1) J_\nu$	$S_\nu \sim J_\nu$
Maxwell distribution is valid	Maxwell distribution is valid	Maxwell distribution is valid
Boltzmann equation is valid	Boltzmann equation is valid	Boltzmann equation is not valid
Saha equation is valid	Saha equation is valid	Saha equation is not valid
Planck radiation is true	Planck radiation is not true	Planck radiation is not true
$P_{gas} \gg \frac{E_{kin}}{Vol}$	$P_{gas} \sim \frac{E_{kin}}{Vol}$	$P_{gas} \ll \frac{E_{kin}}{Vol}$
Total redistribution	Partial redistribution	Partial redistribution
Plane parallel geometry is valid	Plane parallel geometry is not valid for giants	Extreme non-plane parallel geometry ($R_{chr} \gg R_*$)

Table 1.1.: Differences in physics between photosphere and chromosphere.

1.4.2. Chromospheric lines

Since the chromosphere is a very thin layer (in terms of density), it can only radiate in the very strong emission lines. The most prominent characteristic lines of a chromosphere are H_α, Mg II (h+k), and Ca II (H+K). First spotted by Joseph Fraunhofer in 1814, the resonance doublet lines[4] H and K of singly ionized calcium at 3,968 Å and 3,933 Å, respectively, are the deepest and broadest absorption lines in the visible solar spectrum; K being more representative since the H line can be affected by surrounding atomic lines. Further more, both of them can be used as a tool of spectral classification, as they are characteristic for late type stars.

Both of them (H+K) are the only resonance lines in the visible solar spectrum produced by an ionized abundant element (Linsky and Avrett, 1970). In addition, their line formation process takes place in the upper photosphere and lower chromosphere, so they allow us to study such an important region in more detail. For cool stars, emission at the center of these lines can be seen in areas surrounding magnetic features, like sunspots.

In most of the stars whose spectra are known to show Ca II features, the emission tends to be weaker than the continuum spectrum outside the absorption wings. This emission represents chromospheric radiation, while the absorption is produced by the upper zone (or last strata) of the photosphere. But in general, the center of a line is formed at cooler and higher regions in the atmosphere, while the wings depend on hotter and deeper layers (see figure A.1).

A main difference between spectral lines produced in the photosphere and in the chromosphere is that the latter produces emission lines instead of absorption lines. This can be easily explained in terms of the temperature profile of the atmosphere: along the photosphere and in an outward direction, temperature decreases until a minimum temperature value, that indicates the beginning of the chromosphere, is reached as shown in figure 1.3. Since the emitted radiation from the inner photosphere have to pass through cooler gas to reach us, the atoms of this gas will create absorption lines.

On the other hand, when they traverse the inverted temperature gradient of the chromosphere which have low density, we will get emission lines in the spectrum. A good example of this is illustrated in figure 1.4, where the aspect of the H_α line varies with the position of the measurement relative to the center of the Sun. In particular, the Ca II H and K emission lines have been studied by several authors, and Linsky and Avrett (1970) gave a good extensive description of their observational features focused in the solar case.

[4]Spectral line caused by a transition between the ground state and the first energy level of an atom.

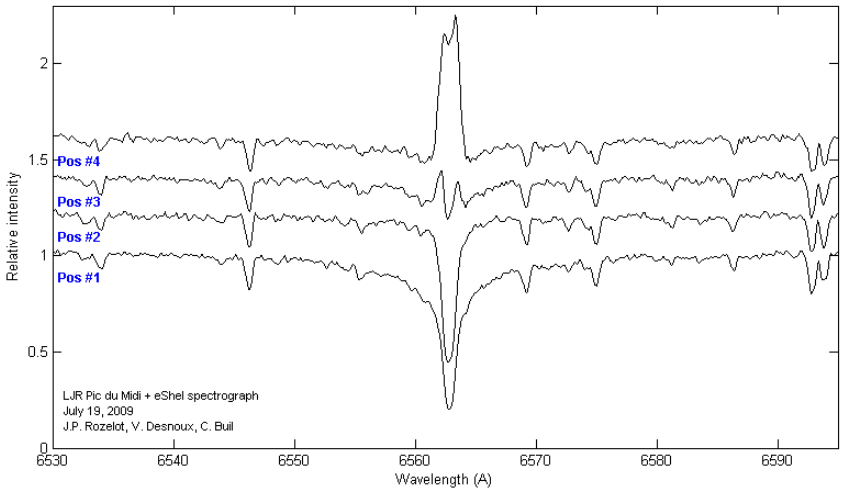

Figure 1.4.: Aspect of the solar H_α emission line relative to the position of the measurement in the solar disk; the numbers indicate greater distance from the center, Pos #1 corresponds to the center of the solar disk and Pos #4 to the outer zone of the chromosphere. Taken from observations of Jean-Pierre Rozelot in the Pic du Midi observatory in 2009.

These aspects can also vary with other physical parameters like temperature, amount of present atoms or gravity. The effects of surface gravity can be visible in stellar spectra, specifically, in their lines. At a given temperature, a line will be more pressure broadened if the surface gravity is larger. Pressure broadening refers to the increase of spectral line widths caused by collisions between the atoms that produce the lines.

The equivalent line width (W_0) is a very common quantity used to describe spectral lines and it is useful to compare their strengths between each other. Its definition is given in terms of the fluxes at the continuum (F_0) and at the line (F_λ) as follows

$$W_0 \equiv \int_a^b \left(1 - \frac{F_\lambda}{F_0}\right) d\lambda \tag{1.13}$$

where the interval $\bar{ab}$ should cover those wavelengths for which $1 - \frac{F_\lambda}{F_0}$ is different from zero. To measure it, one must first calculate the area of the spectral line with respect to the continuum level and then replace the line profile with a rectangle of same intensity and area; the width W_0 of such rectangle corresponds to the equivalent line width (see figure 1.5).

In the figure, the upper panel represents a case where there is a continuum for reference but this is not the case for pure emission lines. Hence, the presence of the continuum

as a reference indicates there should be absorption as well, which turns into a problem since emission and absorption start mixing. It is logical to think then, that the respective equivalent widths will also be mixed and the components may be cancelled.

Therefore, if the concept of equivalent width cannot be applied, one needs to model and work with the entire profile of the lines just as in the case of calcium lines.

But the shape of spectral lines do not depend only on broadening processes related to the abundance of the elements, but also on the details of photon absorption in terms of the amount of matter encountered along the way (i.e., the column mass density) and on scattering.

The column mass density is given by the amount of mass of a certain specie present along a path. It has units of mass over area and its expression is

$$\sigma = \int_a^b \rho(z)dz \tag{1.14}$$

where ρ is the volumetric mass density and z represents a height direction.

If we increase the amount of present atoms, the intensity of pressure broadening will increase as well. This results in a growing line width that can be so important to even contribute to the wings of lines, see figure 4.1(b).

Of all these parameters, the most relevant and important one for this work is with no doubt surface gravity. The mentioned H and K lines have the particularity of varying their line widths with different surface gravities, an effect known as the Wilson-Bappu relation. This phenomena has been studied over the past $\sim$ 60 years and numerous observational evidence is available in the literature, but it has never been fully reproduced neither quantitative chromospheric models exist so far.

The current work aims to revisit, reproduce and improve the calibration of the Wilson-Bappu effect, described in chapter §2, with models of inactive chromospheres of different gravities. Chapter §3 is dedicated to illustrate the generalities of the stellar and planetary atmosphere code PHOENIX, which is used to compute the synthetic spectra needed to measure the Ca II K width lines.

In chapter §4, the methodology of this work is described and the results are presented, which are discussed in §5.

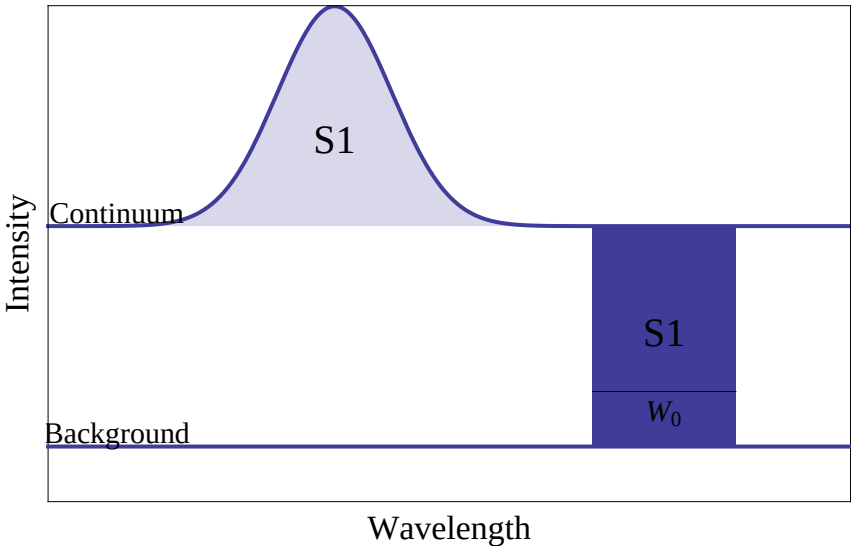

(a) Equivalent line width measurement for emission lines

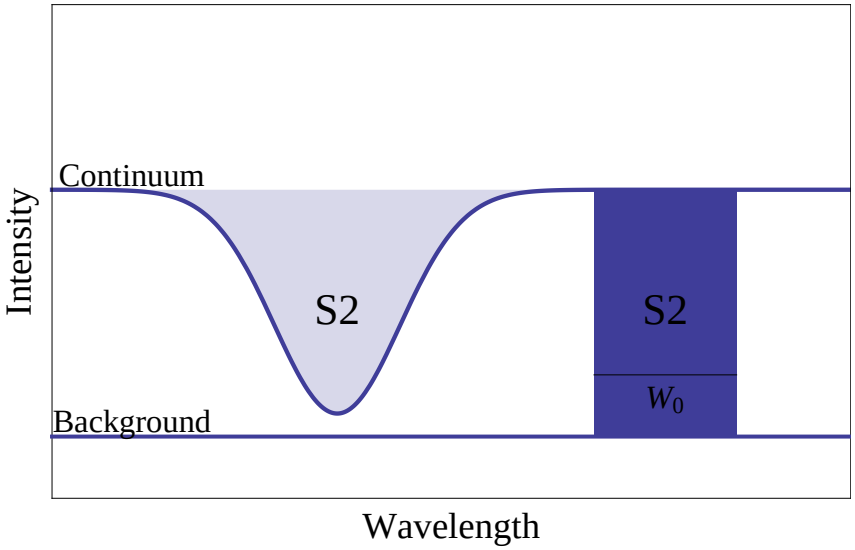

(b) Equivalent line width measurement for absorption lines

Figure 1.5.: Equivalent line width of spectral lines. Wavelength and intensity are given in arbitrary units. The background level represents a value of zero intensity.

2 The Wilson-Bappu effect

2.1. Discovery and history

The Wilson-Bappu effect is a remarkable empirical relation between the width (W_0) of the K emission line of Ca II and the absolute visual magnitude (M_V) of late-type stars. It was first discovered by O.C. Wilson and M.K. Vain-Bappu in 1957 (Wilson and Bappu, 1957) while doing high dispersion spectral analysis.

To achieve this, they used 185 spectra of late type stars of which about 24 spectrograms of 10 Å/mm dispersion were taken a few years earlier with a coudé spectrograph at the Mount Wilson Observatory, located at Pasadena, California. Further observations were included into the sample in order to have homogeneous material. All the stars in the final sample had spectrograms made at Mount Wilson or at Palomar Observatory.

The line widths were measured for stars of spectral type G, K, and M , taking care of discard underexposed plates. Then they were corrected for instrumental width; in general, line widths ranged between $33 - 39$ km/s and 15 km/s were subtracted from each one to account for this correction. When their logarithms were plotted against the respective visual absolute magnitude[1], a defined straight line was found (figure 2.1).

[1]Based on the Yerkes absolute spectroscopic magnitudes.

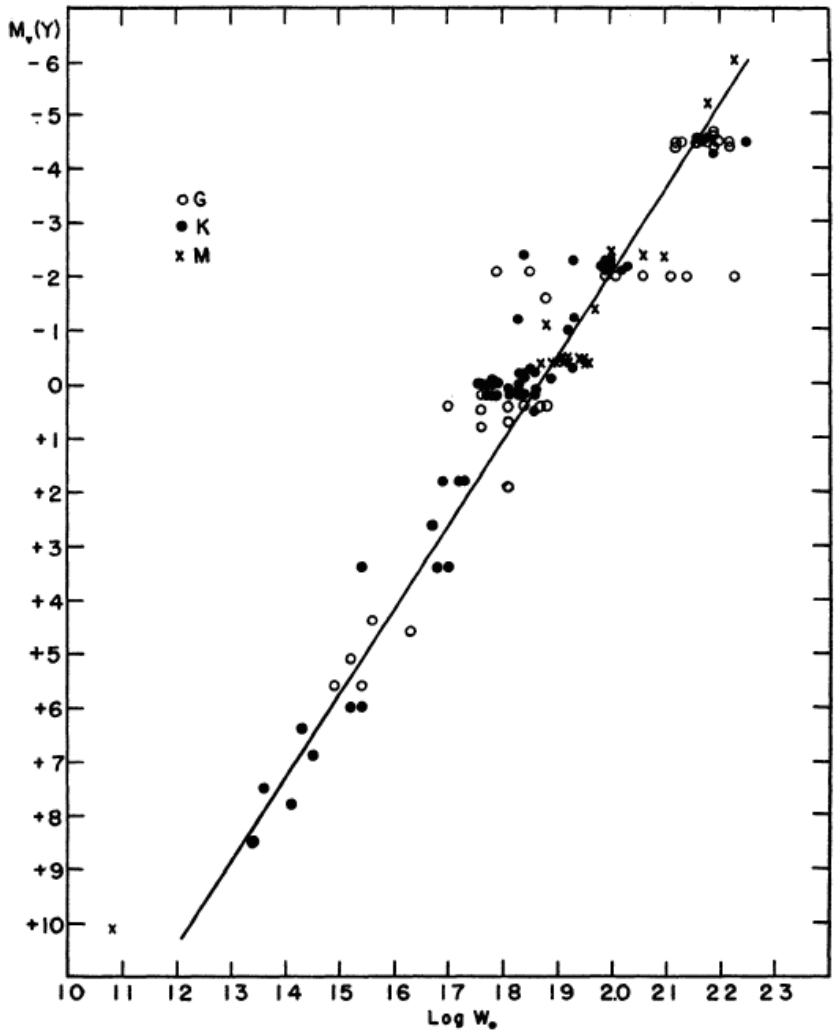

Figure 2.1.: K line widths plotted against Yerkes' M_V by Wilson and Bappu (1957). The solid line is the best linear adjustment drawn by eye and the dashed ones indicate $\pm 10\%$ error in the measurement of W_0. This plot includes all the stars in the original sample, distinguished by spectral types G, K, and M.

Even though at the time no theory relating M_V and W_0 was available, Wilson and Bappu (1957) found the width of the K emission line to be determined solely by the absolute magnitude of the star, being independent of spectral type (and hence effective temperature), intensity, and valid over a 15 magnitud range:

$$W_0 \propto L^{1/6} \tag{2.1}$$

where L is the luminosity of the star. Ten years later this relation was derived by Wilson (1967) using a sample of *Hyades* to be that in equation (2.2). Further work also shows this line width to be independent of the intensity of the K reversal (Zirin, 1971),

and of metallicity (Gómez, 2012).

$$M_V = -14.89 \log W_0 + C \tag{2.2}$$

Such line is the widest and deepest absorption line in late type stars. Since it is very representative of chromospheres, the modern study of the latter is based on it, as well as on the H emission line, both which appear as double reversed emission lines.

A few more efforts to ameliorate this relation and diminish its errors found it difficult to accomplish because of the lack of precise parallaxes back in the date (before *Hipparcos* database), methods for widths measurements and chromosphere models. However, more than four decades later, Pace et al. (2003) made an improvement of the calibration with high resolution spectra while digging into the possibility of use the WB effect as a method to determine accurate stellar distances, which has always been one big problem in astronomy, and concluded the relation (2.3) is followed.

$$M_V = -18.0 \log(W_0) + 33.2 \tag{2.3}$$

This was possible thanks to the accurate measurements of *Hipparcos* parallaxes; similar studies by Wallerstein et al. (1999) and Gómez (2012) indicate that it is possible to calibrate such relation from parallaxes and that it is insensitive to metallicity, respectively. Distance determinations for high luminosity stars are among the most popular applications of the WB effect: observing emission line widths leads to absolute magnitudes, which set distance constraints.

In the present work, I intent to relate the line widths of Ca II K to the basic quantity gravity. There are previous attempts to do this, as that by Reimers (1973), who got the first empirical approach to the dependence on gravity, arguing that M_V is not a fundamental stellar parameter and that if W_0 depends on luminosity ($L \propto \frac{m}{g} T_{eff}^4$), it should also vary with gravity and T_{eff}. He took observations, converted the luminosity dependence into gravity dependence and came up with relation (2.4a), which is roughly the same as (2.4b), obtained by Park et al. (2013) forty years later, who extended the WBR to be an excellent indicator of surface gravity for late type stars.

$$W_0 \propto g^{-0.20 \pm 0.02} \tag{2.4a}$$

$$W_0 \propto g^{-0.17} \tag{2.4b}$$

On the other hand, Ayres (1979) who already knew that the exponent on gravity had to be small (~ 0.20), was working from first principles, from theory only and he arrived to the conclusion that the WBR must be a consequence of hydrostatic equilibrium rather than chromospheric dynamics, i.e., *"The thickening of stellar chromospheres with decreasing surface gravity implies a broadening of the base of the emission core in effectively thick lines such as K..."*. In other words, he established that the WB effect is a consequence of surface gravity of the star.

In general, this is a topic that has fascinated everybody in the field of chromospheres of cool stars over the last (almost) 60 years, including the experts such as Wilson (1967) himself, Ayres (1979), Linsky and Haisch (1979), and Reimers (1973), and obviously the reason is that this expresses fundamental physics of chromospheres. Nonetheless, these methods are purely observational and a theoretical approach with chromosphere modeling has not yet been made.

2.2. Physics of the WBR

The K and H lines of the doublet Ca II are located at 3,933 Å and 3,968.5 Å, respectively, and they are produced at the very bottom of the chromosphere, where temperatures oscillate around 4,000 K (Vernazza et al., 1973). They are then, a special feature of chromospheres and serve as a probe to study their physical properties.

These lines are very opaque with line center optical depths of the order of 10^7 in the photosphere and 10^4 at the temperature minimum (Linsky and Avrett, 1970). For giant stars it is easier to measure them in late life stages: as a MSS passes to the giant stages its radius increases, and if we follow $L \propto R^2$, its luminosity will increase as well making the Ca II K emission line feature get stronger. Thus, the WB effect is more feasible to be measured in late type stars, which in addition, have more magnetic activity in the chromosphere. Activity, metallicity, effective temperature, and column mass density are the most explored parameters in relation with the Wilson-Bappu effect.

The effects of metallicity ($[Fe/H]$) on the WB effect have been studied by several authors too, beginning with Wilson and Bappu (1957), who did not find any dependence on $[Fe/H]$. Later on, Dupree and Smith (1995) noted a diminished line width for stars with $[Fe/H] \leq 2.0$, and Pace et al. (2003) showed the WBR was valid when this value is not lower than ~ -0.4. But the parallaxes used by the first lacked of accuracy due to distance and the findings of the laters was too subtle. With *Hipparcos* parallaxes and data from two globular clusters, Gómez (2012) demonstrated that the WB effect is insensitive to metallicity.

Another interesting parameter to mention is effective temperature. Although the term

T_{eff} appears in some of the derived *generalized* equations of the WBR (Reimers, 1973; Neckel, 1974; Ayres, 1979), the found dependence on effective temperature of W_0 is rather small: $W_0 \propto T_{eff}^a$ with $1.3 \leq a \leq 1.7$. An explanation of such a small dependence is that since W_0 is related with luminosity (as observational evidence indicates), there will be a dependence on T_{eff} because $L \propto \frac{m}{g} T_{eff}^4$. Hence, when using the last expression to relate W_0 with g, the temperature dependence will take place automatically. But if we take a different approach and relate W_0 with visual magnitudes, as Reimers (1973) did and as most authors do, we will be making use of bolometric correction (BC) which depends on effective temperature as $BC \sim -5.4 \log(T_{eff})$:

$$\begin{aligned}
\log W_0 &= AM_V + B \\
&= A\left(M_b - BC(T)\right) + B \\
&= -2.5A \log(L) - ABC(T) + B \\
&= -2.5A \log\left(R^2 T_{eff}^4\right) - ABC(T) + B \\
&= -2.5A \log\left(R^2 T_{eff}^4\right) + 5.4A \log(T_{eff}) + B \\
&= -5A \log(R) - 10A \log(T_{eff}) \mathbf{+5.4A \log(T_{eff})} + B
\end{aligned} \tag{2.5}$$

This means that when we convert the WBR in terms of M_V, as described above, we need a large BC for cool stars that gets even larger for cooler giants.

In other words, T_{eff} takes place in the original relation of line widths ($W_0 \propto L^\alpha$) but it disappears when using the form $M_V \propto log(W_0)^\beta$ as the bolometric correction compensates (bold term in equation (2.5)) the effect of temperature for cool stars.

Column mass density in the chromosphere is also related to the width of such line because it is so optically thick that the increase of its width corresponds to an increase in column density in the chromosphere. Ayres et al. (1975) analyzed seven high resolution stellar spectra and reached to the conclusion that K width–luminosity relation can be attributed to the variation of column mass density with gravity. Their measurements led to

$$M_V \sim -(12 \pm 2) \log W_0 + C \tag{2.6}$$

And applying the bolometric correction to M_V described above they were also able to find

$$W_0^* \propto g^{-0.27 \pm 0.04} T_{eff}^{1.4 \pm 0.2} \tag{2.7}$$

where W_0^* is half of the distance between the minimums of the K doublet. Although in equation (2.7) W_0^* has a dependence on T_{eff}, it can be ignore among F to K stars because the difference between them in T_{eff} (around 50%) is small compared with the difference in surface gravity ($\Delta \log \sim$6.0).

Furthermore, Ayres et al. (1975) suggested how the chromospheric physics may work by arguing that the WBE can be attributed to the variation of column mass density (cm) with gravity (g). First of all, they used hydrostatic equilibrium to relate column mass density with gravity as:

$$P_e \propto g \cdot cm \tag{2.8}$$

where P_e is the electron pressure. But since $\kappa \propto P_e$, with κ being the opacity, then we can write

$$\kappa \propto g \cdot cm \tag{2.9}$$

which by integration over cm leads to $\tau^* \propto cm^{*2} g$. The quantities marked with * indicate the parameters have been evaluated at the temperature minimum. Then they use the argument that all chromospheres have the same continuum optical depth at this temperature minimum, meaning τ^* is independent of gravity. This final and strongest assumption conducts to the following relation:

$$cm^* \propto g^{-1/2} \tag{2.10}$$

In addition, if we use the fact that density n goes as $n \propto g^{1/2}$, then the scale height can be written as $h_0 = cm/n$ which is proportional to g^{-1}, just as in equation (1.10).

In order to relate W_0 with gravity, they use the line profile for damping wings, i.e. Lorentz's profile, ignoring van der Waals broadening and just taking into account pressure broadening to get the relation in equation (2.11). This is possible because the K minimum feature is formed in the damping dominated part of the line profile, and it is known to appear in the region of the temperature minimum where $\tau \sim 2/3$.

$$\tau^* \propto cm^*/W_0^2 \tag{2.11}$$

Taking this value for τ and the result in equation (2.10), we can finally relate W_0 with gravity as:

$$W_0 \propto g^{-0.25} \tag{2.12}$$

On the same grounds, Avrett (1972) compared a solar model with a second one of effective temperature similar to that of the Sun and $\log(g) = 2.0$. Based on the thickness of their chromospheres and optical depths at the region where the K line is formed, he was able to conclude that the atmosphere with lower gravity is less dense but since it is geometrically extended to a greater degree, the outer layers have greater optical depth.

This directly leads to a greater line emission width and the geometry produces greater luminosity. But luminosity is related to gravity as $L \propto g^{-1}$, hence, the width W_0 increases with decreasing gravity. His model also resulted in quantitative agreement with the width-luminosity relationship in equation (2.1) first observed by Wilson and Bappu (1957).

The Mg II k line at 2796 Å holds similar excitation conditions than those of the K line, meaning that the relation between their line widths and other stellar parameters is qualitatively equivalent to those of the K line. Hence, the WB effect is also valid for the k line but since it is located in the ultra-violet regimen of the spectrum it cannot be observed with ground based telescopes, making observations in these line rare and harder to study than the K line. However, Kondo et al. (1972) used a balloon telescope to perform spectroscopy of the Mg k line and showed their line widths are in average ~ 0.4 times wider than those of the Ca II K line and that the WBR is also followed.

As determined by Kraft et al. (1964) while studying the possibility of the use of the H_α line as luminosity indicator, a weaker but analogous correlation can also be seen in this line among G and K type stars.

3 The PHOENIX code

PHOENIX (Hauschildt and Baron, 1999) is a state-of-the-art stellar and planetary atmosphere code that was designed as an *extremely* general code and which has been steadily improved over two decades. It can calculate atmospheres and spectra of stars all across the HRD like main sequence stars, giants, white dwarfs, stars with winds, TTauri stars, novae, supernovae, brown dwarfs, AGN disks and extra solar giant planets (including irradiation).

An example of a solar spectrum computed with PHOENIX is shown in figure 3.1. It has $T_{eff} = 5,780$ K and solar metallicity.

SNIRIS was an early version of this code, which has been renamed and developed within the theory group of the Hamburg Observatory. Since it suffered a lot of major changes, it is said to have *risen from the ashes* instead of being a new version. And so, that is where its name comes from. A general description of the latest version of the code can be found in Baron et al. (2003).

Although some of its parts are written in `C` and `C++` thus there is access to advance and precise arithmetic libraries like `QDA`, PHOENIX is a parallelized `Fortran 95` code. If the implementation of parallel computing is wished, it is necessary to use MPI. Initially, MPI ran on distributed memory architectures, but with the change of architectures in computers, now can also run on shared memory architectures, where several processor have access to a global memory, see figure 3.2. This allows data to move from the space of one process to that of another, undertaking the parallel programing model.

Currently, PHOENIX is supported by several systems including `LINUX` and `Mac OS`; it is not and it will not be supported by any `Microsoft Windows` platform. Documentation, features and *brief* manual of the code are available online to download.

In this chapter I will describe the methods implemented to solve the RTE, which is the basis of PHOENIX, the most important parameters as far as this work concerns, and the

general structure of the code.

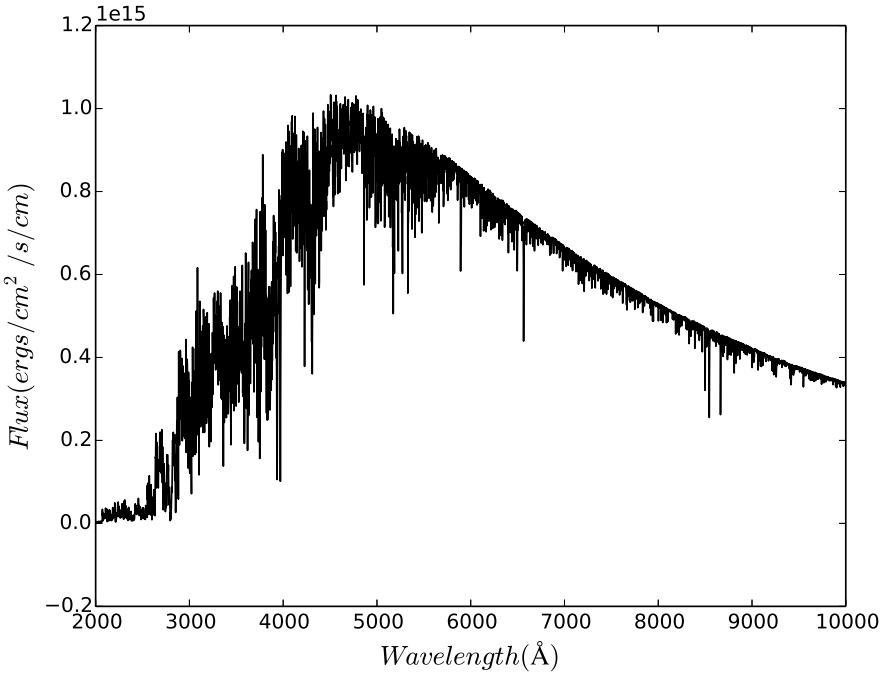

Figure 3.1.: Solar synthetic spectrum.

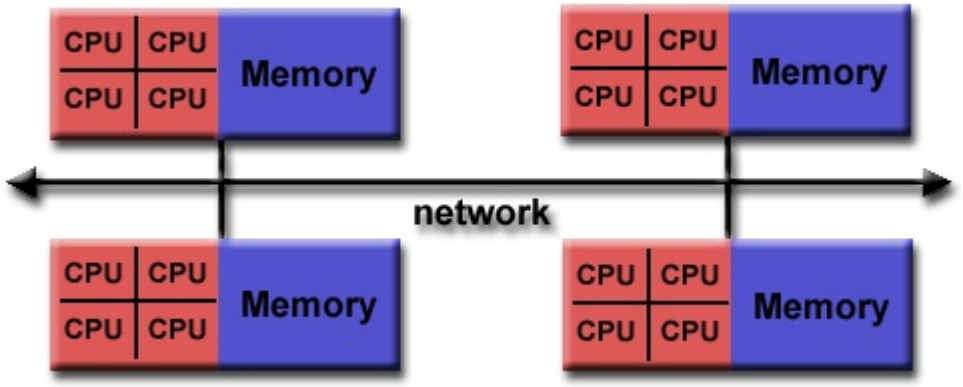

Figure 3.2.: Scheme of a shared memory architecture. Taken from computing.llnl.gov

3.1. Equations and numerical method

Radiation makes the physical properties of an atmosphere, in fact of the entire star, be measurable because the spectrum we see typifies them. But this radiation might change if it passes through matter since more energy can be added or subtracted, phenomenons known as emission and absorption, respectively (see A.1). This means radiation varies with depth in the atmosphere, which makes it essential to model stellar atmospheres. Furthermore, the spectrum of a star can be calculated from such model.

Hence, to model an atmosphere a solution of the radiative transfer problem must be found, i.e., a known source function. PHOENIX does this by applying the short-characteristic method (Olson and Kunasz, 1987) in which a two-level atom with complete redistribution is considered and where the frequency independent line source function is written as

$$S = (1 - \epsilon)\bar{J} + \epsilon B \tag{3.1}$$

where ϵ is the destruction probability, $\bar{J}$ is the mean intensity of a line and B is the Planck function. A full derivation of (3.1) is given in A.2. $\bar{J}$ can also be expressed as ΛS, where Λ is the lambda operator that can be represented as a matrix operator acting on $\bar{J}$.

An iteration method is now used to iterate lambda so we can approximate a source function S^{n+1} from the radiation field produced by S^n:

$$S^{n+1} = (1 - \epsilon)\Lambda S^n + \epsilon B \tag{3.2}$$

The idea of this method is a repeated application of equation (3.2) to eventually reach convergence to the correct solution, but it does not work for small values of $\epsilon(\epsilon \ll 1)$. $\epsilon = 0$ has as solution a grey atmosphere[1] but it also implies that $J(\tau = 0) \ll B$ because if $\tau \ll 1/\epsilon$ (being $1/\epsilon$ the thermalization depth) a photon has a chance to escape through the surface, causing $J < B$.

To ensure thermalization, photons have to be scattered $1/\epsilon$ times, traveling a large optical distance without being destructed. This means they will couple different regions of the atmosphere.

Due to the problem described above, to solve the radiative transfer equation for all wavelength points, the OSI method is used, which is the most commonly used. This method uses spherical symmetry for 1D given by layers or shells and parallel geometry when selected; spherical geometry is useful for extended photospheres, like in giant stars.

[1] Approximation in which the absorption coefficient does not depend on frequency.

To quantify the number of ionized atoms, the Saha equation is included in PHOENIX for more than 3,900 NLTE electronic energy levels and 47,000 atomic transitions (primary lines).

The elements included, along with their respective more important ionization stages, in the EOS used in PHOENIX are H, He, Li, Be B, C, N, O, F, Ne, Na, Mg, Al, Si, P, S, Cl, Ar, K, Ca, Sc, Ti, V, Cr, Mn, Fe, Co, Ni, Cu, Zn, Ga, Kr, Rb, Sr, Y, Zr, Nb, Ba, and La (Allard and Hauschildt, 1995). Dust grains and molecules can be incorporated, but they are only used in this work to model the photospheric emissions and not the chromospheric part due to their high temperatures. Around 300 molecules are included in every model.

More information about the Saha equation and the EOS can be found in A.3.

In addition, the iterative method allows temperature corrections to achieve energy conservation in the equations, as well as radiative and hydrostatic equilibrium.

3.2. Parameters

The most important input parameters for us are those who define the structure of the star and, therefore, the shape of its spectrum. PHOENIX needs at least three of them, which are effective temperature (T_{eff}), a value of surface gravity ($\log(g)$) and mass or luminosity. As an alternative, the radius can also be used. If more than three parameters are given in the scheduler script (see §3.3), all of them have to go in accordance; otherwise, only those most important will be taken into account for the model, but T_{eff} is always a must.

These and other relevant control parameters are describe below.

- **`cmtdis`** Array containing the step size between points in Å. The points are divided in 6 section from 10 to 10^7 Å, each of one can have its own `cmtdis`.
- **`inlte`** Integer variable. Set to 0 for LTE calculations or to 1 for NLTE calculations. When `inlte`= 1, the wanted species must be additionally selected.
- **`logg`** Logarithm of the surface gravity value in *cgs* units.
- **`mass`** Mass in solar masses.
- **`n`** Exponent of the power law density profile given by $\rho(r) = \rho_0(r \setminus R_0)^n$; `n` is an integer. Other density profiles like exponential or arbitrary are also available.
- **`teff`** Effective temperature of the star in Kelvins.
- **`z`** Scaling factor for metal abundances describe by $\log_{10}(z) = [(Fe/H)/(Fe/H)_\odot]$.

As stated before, T_{eff} is one of the most important parameters while modeling a photosphere owing to the fact that it will determine the intensity of emitted radiation, and hence the shape of the spectrum including its maximum emission peak. The latter is established by the Wien's law:

$$\lambda_{peak} T_{eff} = 2.89810^{-3} m \cdot K \tag{3.3}$$

where λ_{peak} is the wavelength at which the spectrum has its maximum emission in meters. As a consequence, shapes of synthetic spectrum will be regulated by the so-called parameter (see figure 1.2) and must not be overlooked. Furthermore, the appropriate selection of spectral types is also dependent of it.

On the other hand, surface gravity is in charge of the internal structure of stars. In PHOENIX, there is a model for dwarf's atmospheres where plane parallel geometry is assumed and gravity is the same for all radial points. But since giant stars have an extended atmosphere, this is not be suitable for them and so an alternative is a second model for stellar atmospheres specially used for this type of stars, which uses spherical radiative transfer and where gravity does not remain constant but changes with radius instead. Therefore, the choice of the right model mostly lies in the value of surface gravity.

For stars with reasonably high surface gravities ($\log(g) > 3.0$), the atmospheres have a relative extension of less than 1% and they can be handled with plane parallel approximation (Allard and Hauschildt, 1995). Nonetheless, in this work I have limited all models to spherical symmetry, which is translated as an atmosphere constituted by layers or shells. Each of such layers is required to follow the equations mentioned in §3.1 and continuity between them is also a must. The effect of gravity is also visible in spectra since a line will be more pressure broadened if surface gravity is larger.

Of course, an entire stellar interior is only completely elucidated when all of the quantities involved are taken into account. These quantities are density, gravity, temperature, gas pressure, mass, and luminosity. They constitute the equations of stellar structure which are not be explained here because they are not of fundamental matter to this work.

3.3. Program files

PHOENIX is a considerably large program so it is structured in modules or units that contain different independent subroutines. They can be computed at the same time and when the computations are done, all the information is put together. This characteristic makes possible a parallel computing.

These procedures are written in the main code named `phoenix.f`, which is the "driver" program and consists of almost 25,000 lines describing the entire code.

Besides the main program, there are other program files including the input parameters (see §3.2), ionization potentials, routines with methods to obtain line opacities, for RT and NLTE calculations as well as for atoms and molecules.

In fact, molecular line data is one of the most significative differences and improvements of the code. This was possible with the addition of HITRAN92 database, which back in the time included line parameters for 31 species and 709,000 transitions (Rothman et al., 1992).

The atomic line list, taken from Kurucz and Bell (1995), also plays an important role in this code since it is crucial for the correct interpretation of emission lines. It contains information of 80 million lines that are been used to compute the absorption and emission from spectral lines of $\sim$ 60 species. They are being distributed by R. Kurucz on DVD format to modelers and the newer version is available online.

As its name says it, the scheduler script in PHOENIX is in charge of arranging the jobs within the main program. The principal tasks are (1) reading and writing of the input and output files (or units), respectively, and (2) describe the parameters that define the model. All stellar[2] parameters, temperature corrections details and the set of atomic LTE and NLTE species to be included, are listed here.

Input files are always units containing the structure (optical depth, electronic temperature, column mass density, gas and electronic pressure, radius, etc.) of a previously well converged photosphere with similar parameters of that to be computed. If surface gravity, effective temperature, or mass are too different, the computation of the model will need a larger number of iterations before it reaches convergence. These differences are considered to be large when $\Delta \log(g) > 1.0$, and $\Delta T_{eff} > 1,000$ K; if they are small, an amount of 10 to 30 iterations is enough to reach convergence.

Output units are of the same structure of the latter but they contain the structure of the new model. In addition, a second very important output unit gives the surface flux as a function of wavelength.

Every iteration consists in the reading of the input structure and finalizes with a temperature correction. This is how a final synthetic spectrum is gotten, but in between a lot of steps must be done. First of all, the hydrostatic equation is integrated (here, radiation pressure is ignored for simplicity at the very first iteration because it is unknown), making sure that the equation of state remains valid in each layer of the atmosphere. Then the radiative flux (F_{rad}) is computed also for each layer and the radiative transfer equation is solved for every wavelength point.

At this point, if NLTE is going to be considered, the rate equations (including the

[2]This is, of course, for the stellar atmosphere case. Otherwise, the parameters have to be those of a rapidly expanding atmosphere or a planetary one.

Boltzmann and Saha equations, see appendix A.3) have to be solved. The OSI method is used to solve them.

$$F_{tot} = F_{rad} + F_{conv} = \sigma T_{eff}^4 \tag{3.4}$$

After this, we might find that F_{rad} is not equal to σT_{eff}^4 even when the convective flux (F_{conv}) is ignored (see equation (3.4)). If this is the case, the temperature for each layer has to be corrected trying to get a better convergence, so a new iteration begins with the modified temperature values, which are determined by energy conservation. Essentially, this is repeated until the model has converged or until a specific number of iterations has been reached.

3.4. Photospheric models

Well-tested, accurate photospheric PHOENIX models already exist for cool giants, but these artificially end in the temperature minimum. Hence, all weak and medium photospheric lines are matched excellently. These models encompass the coolest known M dwarf, M subdwarfs and brown dwarf candidates having a wide range of parameters: $5,000$ K$\leq T_{eff} \leq$4,000 K, $3.5 \leq \log(g) \leq 5.5$ and $-4.0 \leq [M/H] \leq +0.5$ (Hauschildt et al., 1996).

But emission from the chromospheres, as observed in the very strongest lines such as Ca II K, caused by the outwardly increasing temperature in the chromospheric layers, has so far been left unconsidered. Due to the fundamental nature of this problem, no quantitative chromospheric models exist so far, neither has the Wilson-Bappu effect (§2) been reproduced to fully match the observational evidence.

4 Method and results

The current chapter is dedicated to describe the methodology of this work, and is not planned to be a PHOENIX user's manual, but it will remark crucial details to take into account while modeling chromospheres. The technical findings of such practice will also be related not as formal results whereas as warnings and guidance for future users in view of the fact that no chromospheric models for low gravity stars exist so far.

This chromospheric mode included in PHOENIX (Fuhrmeister et al., 2005) has been successfully applied in modeling of M dwarf chromospheres (Hauschildt et al., 1996).

4.1. How to compute a PHOENIX chromosphere

To compute a chromosphere with the code package PHOENIX, an executable scheduler script of PHOENIX and an executable of *make_chromos*, which will contain the information about the structure of the chromosphere are needed. *make_chromos.f* is a program file that includes an input file named *chromos.dat* which needs, in turn, a file containing the structure of a photosphere as input, and has a different file as output. The latter will hold not only photospheric data but also those of a chromosphere attached to this particular photosphere.

The input file for *chromos.dat* must be a model produced by a converged and well behaved photospheric simulation; information of how to get this is given in §3.4. It is recomendable to make this simulation with the same desired parameters for the chromosphere like effective temperature, mass, chemical composition, etc. Taking this precaution will avoid a mismatching of both photospheric and chromospheric spectra, otherwise it would be impossible to compare their continuum. A description of the parameters that can cause a significative change in the spectrum with an attached chromosphere will be held in this chapter.

In order to obtain an output file from *chromos.dat*, and hence the structure of the chromosphere, first it is necessary to compile the program file *make_chromos.f* — this is

done within the PHOENIX's BIN folder, where the binary or executable files are located. The output file will carry information that describes the structure of the chromosphere, the aforesaid information is included as variables like the initial temperature value (minimum temperature), the maximum temperature value located at the top of the chromosphere, its turbulent velocity (V_{tur}), column mass density, etc.; they are broken down below in table 4.1.

Parameter	Used values	Units
Temperature at top of the chromosphere	8×10^3 - 10^4	K
Temperature at top of the atmosphere	20,000	K
Turbulent velocity in the photosphere	2.0	km/s
Turbulent velocity at top of the chromosphere	10.0	km/s
Column mass at temperature minimum (log scale)	-2.5	gr/cm^2
Column mass at top of the chromosphere (log scale)	-6.5 – -7.0	gr/cm^2
Outer pressure in transition region	10^{-4}	dyn/cm^{-2}

Table 4.1.: Parameters for the structure of the chromosphere in solar type star models.

The temperature at the top of the chromosphere was set to 8,000 K by Ayres (1979), although a few years early Vernazza et al. (1973) used 8,500 K in their model, saying this value is still lower than the corresponding temperatures, and they used 20,000 K for the top of the chromosphere. Turbulent velocities in the photospheric region of $1 - 2\ km/s$ have been previously used with satisfactory results (Maltby et al., 1986; Houdebine et al., 1995). The turbulent velocity along the chromosphere in PHOENIX is given by a linear function starting at the V_{tur} in the photosphere and ending with the chosen value for turbulent velocity at the top of the chromosphere (V_{tur}^{top}). This value has been proposed to be 8.5 km/s when $T_{eff} = 8,000$ K in a VAL model made by Maltby et al. (1986). After the chromosphere region, a second linear temperature rise is applied to form the TR, which is considered to be the top of the atmosphere.

As with turbulent velocities, the temperature along the chromosphere is given by a linear rise but it is a function of column mass that goes like $T = 7.5 \log(cm)$, where cm is defined as in (1.14) and z denotes increasing distance in the inwards direction. In the upper layers of the photosphere, column mass was set to $\log(cm) = -2.5$, while in the outer zones of the chromosphere it was chosen to go in agreement with hydrostatic formulation such that

$$\log(p_{out}) = \log(g) + \log(cm_{top}) \tag{4.1}$$

For a fixed arbitrary value of $\log(p_{out}) = -4$. Hence, for surface gravities ranging between 2.5 and 5.0, cm_{top} varies from -9 to -6.5 in a logarithm scale. Nonetheless, in most of the cases this was restricted to -7 in order to keep a reasonably extension of the chromospheres and their densities high enough to produce emission lines. It is important to note that varying the computed values of equation (4.1) too much can lead to inconsistencies in the hydrostatic equations of the code and models may not carry on.

After having chosen all these data, they have to be used as an input file for the scheduler script containing the option *ichrom2=t*. Such option activates the chromospheric mode incorporated in PHOENIX. There is also an alternative function *ichrom=t* for the chromospheric mode but it will no be describe here. In addition, the parameter *chvtb_fac* is highly recommended to avoid the chromosphere's turbulent velocity (V_{tur}) surpass the sound velocity (V_S): when computing a chromosphere, an increase of turbulent velocity will be impose and it might be higher than the sound velocity. Using *chvtb_fac* will set the value of V_{tur} to a fraction of V_S all along the chromosphere.

Once all of the above has been done, our final output will include both photospheric and chromospheric emissions. Note that if *non-LTE* is activated, only the specified species will appear in the spectrum and those which are of much interest must be previously selected.

A step by step instructive for the computation of a chromosphere is given below:

1. Get an output file from a scheduler script that does not include the function *ichrom2=t*. It will contain only a structure of the photosphere.

2. Use such file as input for *chromos.dat*, which must contain the desired chromospheric parameters.

3. Compile *make_chromos.f* within the compiler folder contained in BIN.

4. Copy *make_chromos* to the location of the needed files and run it. The output file of *chromos.dat*, containing the chromosphere's structure, should now appear in the same location.

5. Specify this new file as the input file for the scheduler script that includes the function *ichrom2=t* and run it.

6. The final result is a spectrum of the photosphere with a chromosphere incorporated in a semi-empirical way.

Please note and bear in mind that chromospheric parameters for low gravity stars are not obvious and they do not have been previously defined by any other work. Vernazza et al. (1973) proposed values for temperatures at the bottom and at the top of the chromosphere, as well as the respective column mass values for a solar model. Although they achieved a well accepted model, such parameters were only chosen with the goal of being

able to match observations (when available), reproduce a well behaved TR and produce prominent Ly_α lines and, therefore, some arbitrarily data points lack physical meaning.

4.2. Making models

Calculating a good chromospheric model depends on the adjustment of several parameters, besides of having a previously well converged photospheric model to work with. Such parameters define the whole structure of the chromosphere. Those that are of interest for us are the temperature at top of the chromosphere (T_{top}) in K, the column mass density (cm) in gr/cm^3 and V_{tur} in km/s at the bottom and at the top of the chromosphere.

Initiating with a converged solar model, eleven models of chromospheric emission were calculated; they are listed in table 4.2. All of them have the same values of V_{tur}=10 at top and V_{tur}=2 at bottom, but different T_{top} and cm at the bottom of the chromosphere. These models deem as a first test to check whether the mentioned parameters affect the core of the CaII K line noticeably.

All computations have been made with the NLTE mode for the species H I, He I, He II, Ca I and Ca II, with T_{eff} =5,780 K and $M = 1M\odot$. Gravity values are $\log(g) = 4.4$ for models described within this section but they vary in §4.4.

No.	T_{top}	$\log(cm)$
0	8,000	-2.5
1	6,500	-2.5
2	5,000	-2.5
3	9,500	-2.5
4	11,000	-2.5
5	8,000	-4.0
6	8,000	-4.5
7	8,000	-1.0
8	8,000	+0.5
9	8,000	-2.0
10	8,000	-3.0

Table 4.2.: Parameters for the first chromospheric models.

The first models shown that the best temperature T_{top} must be around 10,000 K, where hydrogen absorption is maximized, and that $\log(cm) = -2.5$ builds a better shape of the Ca II K line core, i.e., emission is measurable and wings are not so prominent. In figure 4.1(a), the differences produced by temperature changes with same $\log(cm)$ are shown, and those produced by column mass density with same T_{top} are in figure 4.1(b).

The changes of the maximum temperature at the top of the chromosphere indicate that increasing this parameter will produce more emission of the Ca II K line. Similarly but with a stronger effect due to the logarithmic scale, a higher value of column mass at the bottom of the chromosphere where the K line is formed, is reflected in stronger emission of this line.

Now what remains to be explored is if the chosen turbulent velocities can actually make a difference in the outcomes of the models. With such objective, three more spectra of different V_{tur} were obtained. Their parameters are shown in table 4.3.

Jevremovic et al. (2000), while modeling atmospheres of dwarf stars, found a decrease in electron density with turbulent velocity. Since the Ca II K line formation process occurs in the region of temperature reversal, whose structure is determined by the parameters at the bottom of the chromosphere, the values of V_{tur} at the bottom of the chromosphere (V_{tur}^{bottom}) were not changed to avoid excessive contribution to such line.

No.	T_{top}	$\log(cm)$	V_{tur} **at bottom**	V_{tur} **at top**
11	10,000	-2.5	2	8
12	10,000	-2.5	2	7
13	10,000	-2.5	2	6

Table 4.3.: Parameters for models with different turbulent velocities.

Models 11 to 13 did not present any visible change in their spectra. This can be attributed to the lack of importance of the higher layers of the chromosphere when it is about calcium emission, i.e., the Ca II emission is produced within the bottom of the chromosphere. Therefore, changing the upper turbulent velocity does not affect the bottom enough to be perceived in such line.

4.3. Smoothing temperature profiles

In figure 4.2 the temperature profile corresponding to model #11 is plotted. There, one can clearly see the beginning of the chromosphere at the temperature minimum. From left to right, the abscissa indicates the beginning of the photosphere, where the temperature starts to drop until it reaches a minimum value. After this point and up to the selected maximum T_{top}, the values correspond to the chromosphere's profile. But this function looses continuity at that precise point, which means both curves (from the photosphere and from the chromosphere) are joined but not in a smooth way.

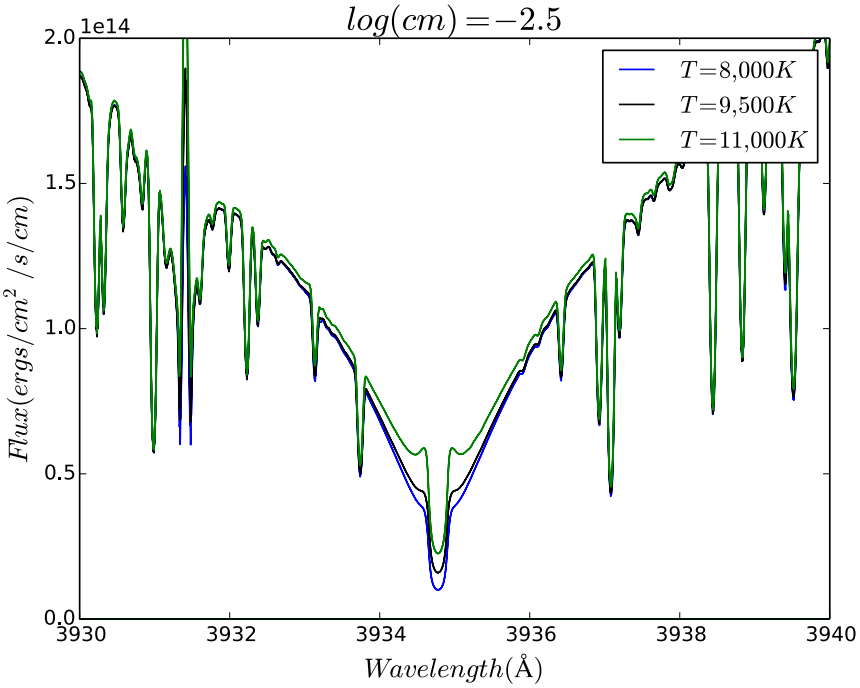

(a) Effects of the temperature.

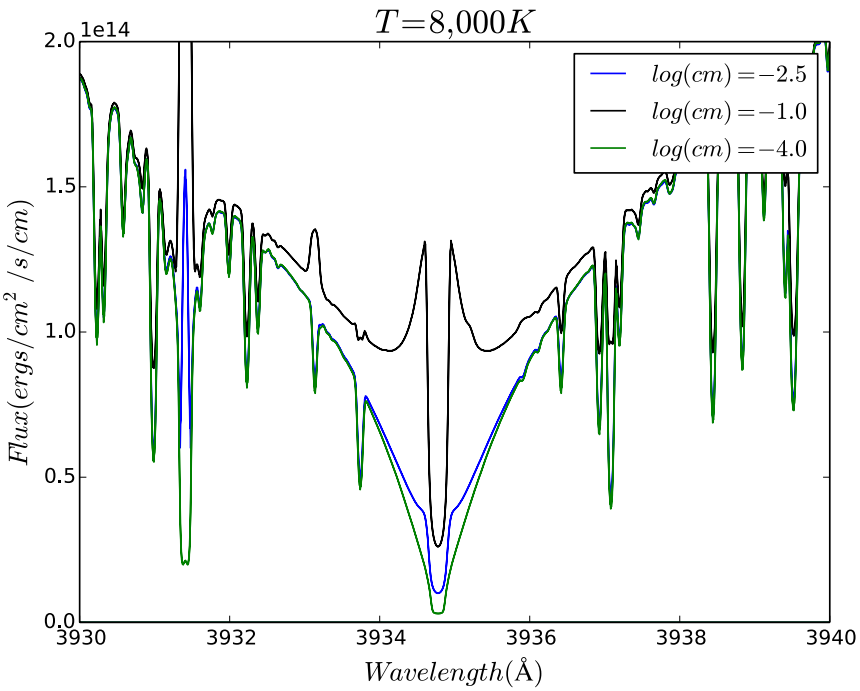

(b) Effect of the column mass.

Figure 4.1.: Effects of temperature at the top and *cm* at the bottom of the chromosphere for solar models.

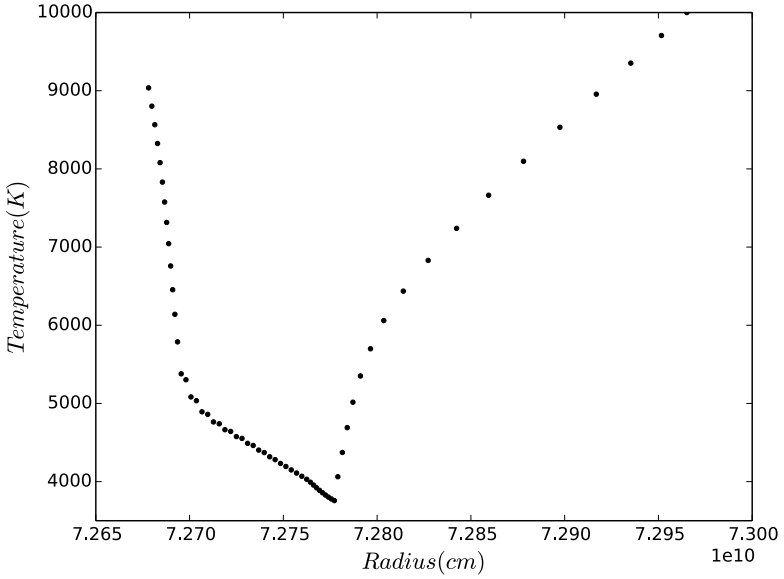

Figure 4.2.: Temperature profile of a solar model.

Physically, this is not what we are expecting, since the photospheric region must be in equilibrium with the chromosphere. This situation can lead to undesirable features in the core of the Ca II K line, such as a very deep core or no signs of emission. To avoid this problem, one must manually change some temperature values of the region surrounding the minimum point and make a smooth curve. Manual changes in temperature can also be helpful when T_{min} is not high enough to produce the desired output. Three spectrum have been made to fix this issue. The complete profiles are included in appendix B.1 and the description of the corrections are as follows:

1. **Flat Valley** There were nine points in the profile with temperature lower than 4,000 K. Their values were arbitrarily increased and set to 4,000 K. With this correction the intensity of the Ca II K line gets smaller, narrower, and the core does not seem to be affected, but still the temperature profile has non-smooth zones.

2. **Symmetric Correction** The same nine points were modified but in a symmetrical manner. The fifth point was set to 3,860 K, those at the edges at 4,000 K, and the remaining were set 35 K apart each. Although a symmetric distribution ameliorates the problem, it is not the best way to do it because going from the minimum point to the photosphere and to the chromosphere does not follow the same function. Imposing this causes the temperature profile to look unnatural.

3. **Smooth Curve** A more accurate profile was found when symmetry is not considerate and a smooth curve is searched instead. The chosen values of temperature are listed below from left to right.

4.000	3.965	3.930
3.930	3.945	3.962
3.980	4.000	4.015

This selection of values makes the line emission core to be less deep in the very center and also produces a narrower line, which we are looking for. In addition, the emission in the wings increases leading to a better define width of line.

All of these corrections along with the original curve are shown in figures 4.3 and 4.4; they display temperature profiles and Ca II K lines, respectively. The photospheric parameters of these models correspond to the inactive Sun, i.e., a Sun with no magnetic activity. Similarly, since the structure of their chromosphere has been chosen to match their photosphere, they represent a Solar one. This entail complete non-active Solar models, which are to be compared with observational data in further work.

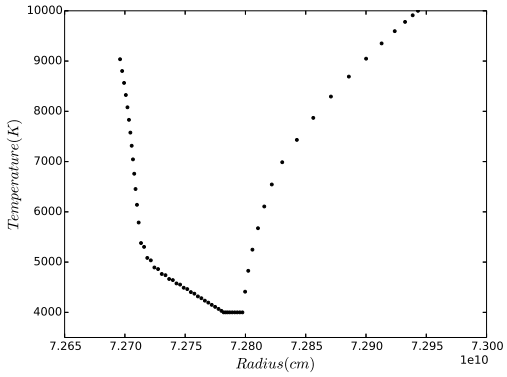

(a) Flat Valley.

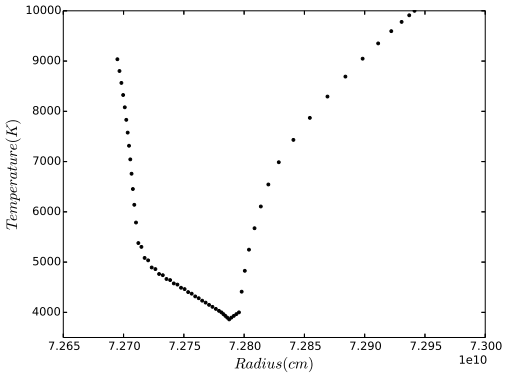

(b) Symmetric Correction.

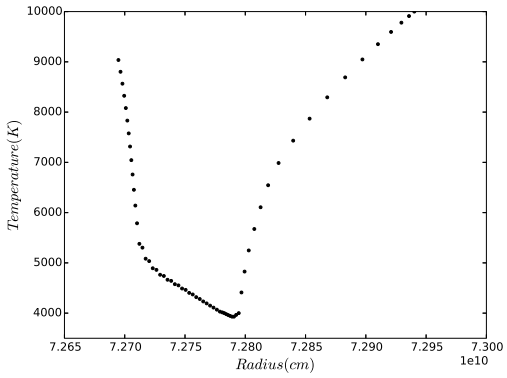

(c) Smooth Curve.

Figure 4.3.: Temperature corrections in the chromosphere for solar models.

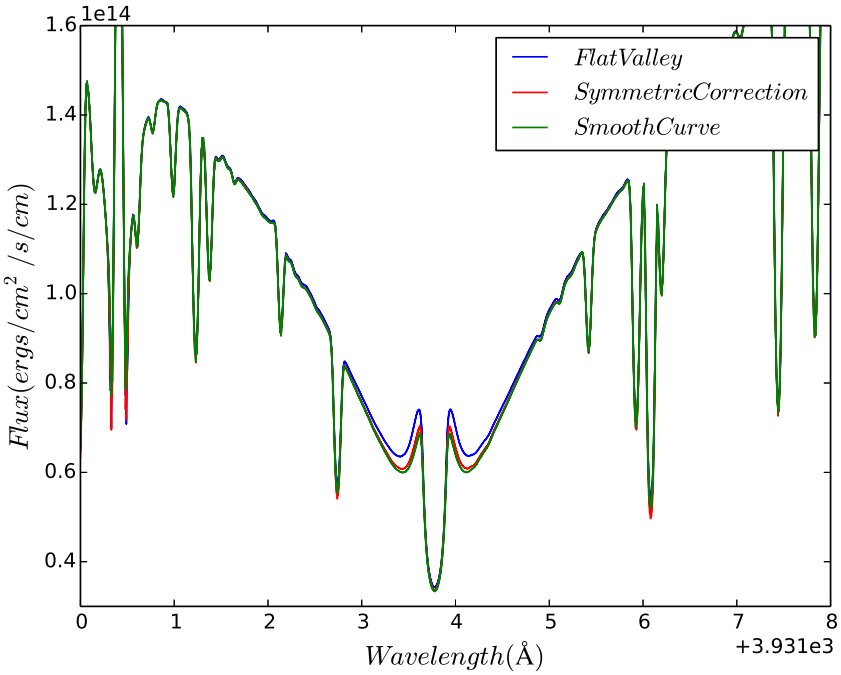

Figure 4.4.: Ca II K for solar models with temperature corrections.

4.4. Changing surface gravity

To compute the chromosphere models for different values of gravity, the same method established in §4.1 has to be applied. But first of all, converged photosphere models are needed. Since we are aiming for them to have different values of gravities, the whole structure of each synthetic star will be different. This is true because hydrodynamic equilibrium is a must for stellar structures, making surface gravity one of the most important parameters for modeling stars.

Hence, if we compare two stars of equal T_{eff} but different surface gravities, their structure will differ more than in the opposite case (same surface gravity but different T_{eff}). This entail a problem when computing such spectra: since the PHOENIX code requires a previously converged model to start a new model with another set of parameters, the convergence and well behavior of the results can depend on the right choice of the parameters of the input file.

For this reason, a big change in gravity between models may not be suitable to compute them one after another. To avoid significative changes in the structure of each model, I have started with a solar model whose logarithm of surface gravity is $\log(g) = 4.4$ and then used it as input for the next ones making steps of only $\Delta \log(g) = 0.1$. This procedure was repeated until $\log(g) = 2.5$ was reached, being all of them LTE models.

Nonetheless, with the latest version of PHOENIX, one should be able to make new photospheric models with changes of about $\Delta \log(g) = 0.5$ without convergence problems due to improvements in the equation of state.

Five out of these models were selected to be used as input for NLTE models keeping all other parameters the same. The chosen ones were those with $\log(g) = 4.4, 4.0, 3.5, 3.0$, and 2.5. A sixth one for $\log(g) = 5.0$ was gotten to extend the data for gravities above the solar value. Then the NLTE models for different gravities served as bases for chromospheric models. Maximum temperature in the chromospheric region was the only parameter (besides gravity) that has been changed in each model, they were set to 10,000 K for $\log(g) = 5.0$ and 4.4, 9,000 K for $\log(g) = 4.0$ and 3.5 and 8,500 K for $\log(g) = 3.0$ and 2.5.

The reason for such thing is high temperatures at the outer layers of low gravity stars do not work because radiation pressure overtakes gravity. Output spectra are shown in figure 4.5, where the differences in flux around the Ca II K line due to the changes in gravity can be seeing.

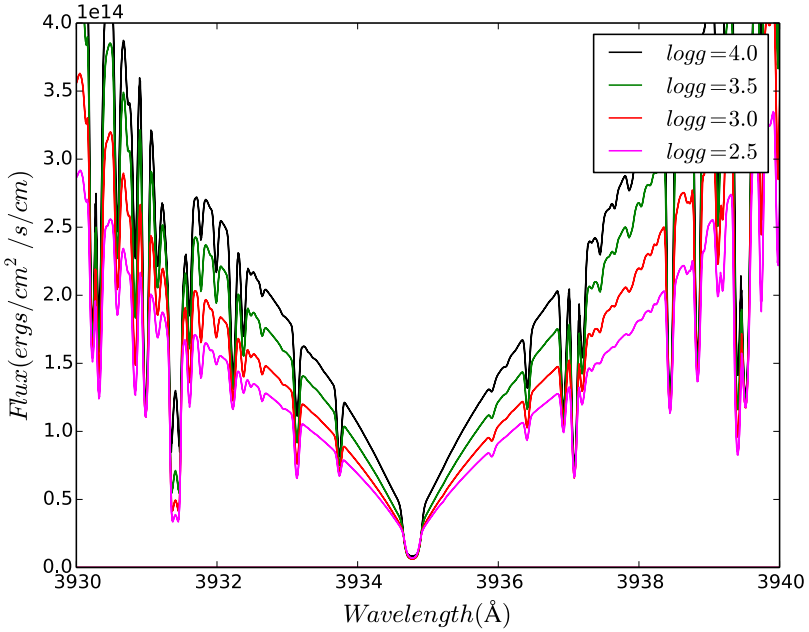

Figure 4.5.: Ca II K line for different gravities.

To get measurable K lines in these models, some changes in their temperature profiles were made. Different values of column mass density were also applied. Such parameters vary from $3,800\ \text{K} \leq \text{T}_{\text{min}} \leq 4,200\ \text{K}$, $8,500\ \text{K} \leq \text{T}_{\text{top}} \leq 10,000\ \text{K}$, and $-5.7 \leq \log(cm)_{bottom} \leq -7.0$. Physical parameters of the best results among them are listed in table 4.4 and the corresponding emission lines are shown in figure 4.6.

This models only include surface gravities from $\log(g) = 5.0$ to $\log(g) = 3.5$, for the two remaining models, measurable emission could not be obtain by the method described in this chapter and the alternatives will be discussed in §5.

$\log(g)$	T_{top} **(K)**	$\log(cm_{top})$ **(gr·/cm^2)**	p_{out} **(dyn/cm^2)**	**R (cm)**
5.0	10,000	-7.0	10^{-4}	3.65×10^{10}
4.4	10,000	-7.0	10^{-4}	7.31×10^{10}
4.0	9,000	-6.6	10^{-4}	1.16×10^{11}
3.5	9,000	-7.0	10^{-4}	2.08×10^{11}

Table 4.4.: Physical parameters for the best chromosphere models, presenting emission of K line, for different values of surface gravity.

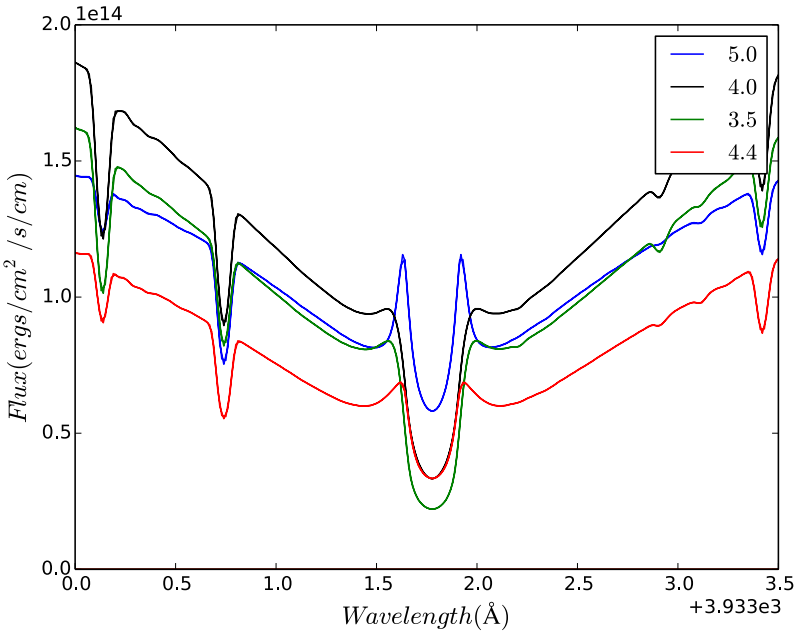

Figure 4.6.: Spectra of the best chromosphere models, presenting emission of K line, for different values of surface gravity. The specified values on the right top corner correspond to the respective values of $\log(g)$.

5

Discussion and conclusions

5.1. Structure of the models

Figures 5.1, 5.2, and 5.3 display the structures of the models for chromospheres with $T_{eff} = 5,800$ K and different surface gravity. The first one shows the logarithm of column mass density in $g \cdot cm^{-2}$, the second is for the gas pressure (P_{gas}) in $dyn \cdot cm^{-2}$, and the third one illustrates the electron pressure (P_e) in same units. All of them are plotted against the electron temperature (T_e) given in *Kelvins*.

The changes in extension of column mass between the different chromosphere models (figure 5.1) are not significative because (1) they were chosen to be consistent with each others, and because (2) densities are so low in the chromospheres ($\log(cm) \sim 10^{-4}$) that the small changes are not significant in comparison with those within the respective photospheres. Nonetheless, *cm* photospheric values present variations consistent with the surface gravity of the models; these values go from a maximum of 9.08 $g \cdot cm^{-2}$ for the model with $\log(g) = 5.0$ to 17.28 $g \cdot cm^{-2}$ for $\log(g) = 3.5$.

The synthetic spectral energy distributions (SED's) of the models are illustrated in figure 5.4. The wavelengths have units of Å and the values of flux correspond to a logarithmic scale, the flux units are $erg/cm^2/s/cm$. As seen in this figure, the usage of LTE atomic lines in the model together with NLTE hydrogen lines causes the hydrogen continuum in the blue, at around 900 Å, to have strong emission lines. Such lines can pump the hydrogen unrealistically towards redder zones of the spectra, spoiling some other NLTE lines like H and K through electron pressure.

A possible solution to this problem is to eliminate all LTE lines off the models, keeping only the selected NLTE species. This will produce rather flat spectrum with only a few lines on them. When this procedure was followed, no difference in the shape or intensity of the K emission lines was observed. Therefore, the original models (with LTE and NLTE atomic lines) were kept.

In figure 5.5, the temperature profiles of the four models are shown. Temperatures are given in Kelvins and radii in *cm*, except for the solar model, where the temperature is a function of height. Here, height is given in kilometers measured above a zero point were $\tau_{5000} = 1$, this to be consistent with the model of Vernazza et al. (1973) in figure 1.3.

Their model has a temperature minimum of 4,100 K located at 520 km, while in this work I use a minimum of 3,930 K at 830 km. Between 1,000 and $2,000$ km, they have adopted arbitrary values of the temperature, making it rise up to 6,000 K; in contrast, this region in the model of figure 5.5(b) corresponds to the central region of the modeled chromosphere with PHOENIX. After $2,200$ km and 8,500 K, they put a second sharp increase of temperature to model the transition region, point that is very close to the end of the chromosphere in this model at $2,342$ km and which does not include a transition region. Although the difference in temperature for this point ending the chromosphere with this work is of 1,500 K, Vernazza et al. (1973) claimed they used a lower temperature than the corresponding to compensate the high-temperature plateau at $2,400$ km.

5.2. Measurement of the lines

The principal aim of the investigation was to see how the emission line widths of the Ca II K line behave as a function of surface gravity in chromospheric models of inactive stars. Different values of surface gravity were selected to compute the models, whose K lines were then analyzed individually. This selection of parameters represents an advantage in the analysis because spectral type and effective temperatures can be controlled.

All the chromospheric models were computed with the same version of PHOENIX (16.05.00D) released on May 22nd, 2013, and with the same OS. This detail may not seem very relevant but it is important to maintain concordance between computations due to changes and improvements of the code that manage different ways of solving the EOS. Also, it has been noticed that models of same structures and parameters can lead to small differences in spectra when computed by different operating systems. Hence, taking this precaution will avoid unwanted differences in the shape of the chromospheric emission lines proper of computational aspects.

Along the same line (Ca II K), the measurements of the K emission line widths were finished before any relation was calculated in order to avoid subconscious bias. Results of the measurements are listed in table 5.1. This methodology was made by two individuals separately, obtaining the same result.

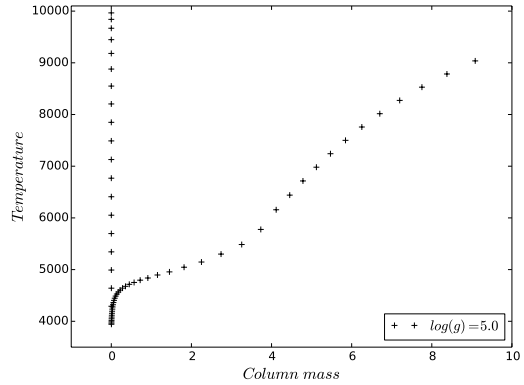

(a) Structure for the model with $\log(g) = 5.0$. The maximum value of cm is 9.08 $g \cdot cm^{-2}$.

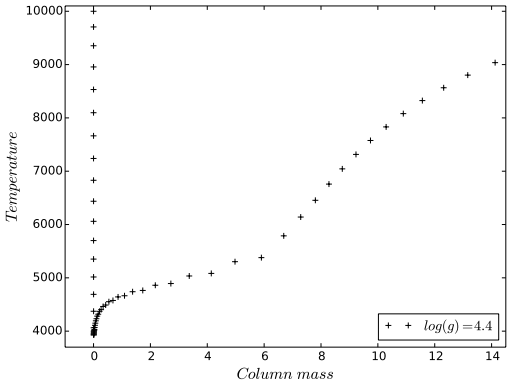

(b) Structure for the solar model. The maximum value of cm is 14.12 $g \cdot cm^{-2}$.

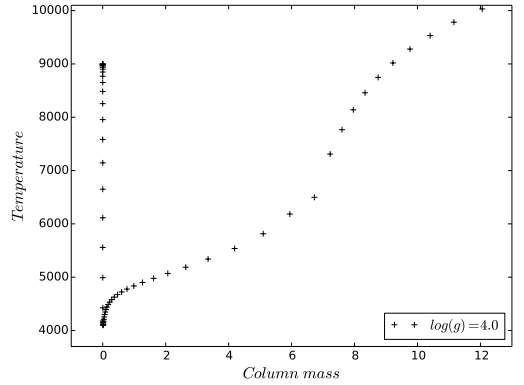

(c) Structure for the model with $\log(g) = 4.0$. The maximum value of cm is 12.05 $g \cdot cm^{-2}$.

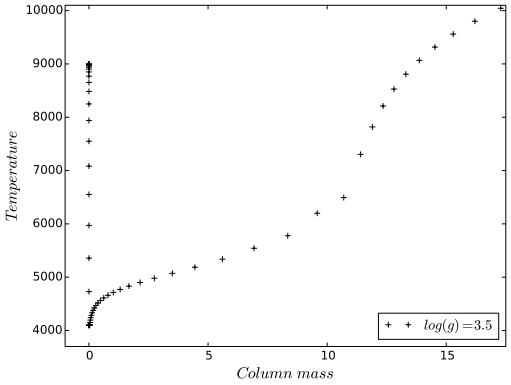

(d) Structure for the model with $\log(g) = 3.5$. The maximum value of cm is 17.28 $g \cdot cm^{-2}$.

Figure 5.1.: Structure of the best models for different gravity. cm is the logarithm of column mass density, which is given in units of $g \cdot cm^{-2}$ and the temperature is the electron temperature in *Kelvins*. From left to right, the points correspond to the chromospheres towards the photospheres. All models have T_{eff} =5,800 K.

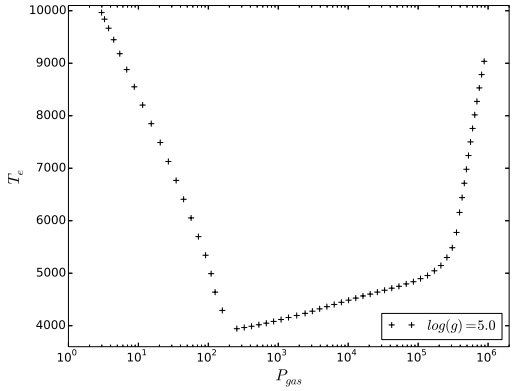

(a) Structure for the model with $\log(g) = 5.0$. The maximum value of P_{gas} is 8.78×10^5 $dyn \cdot cm^{-2}$.

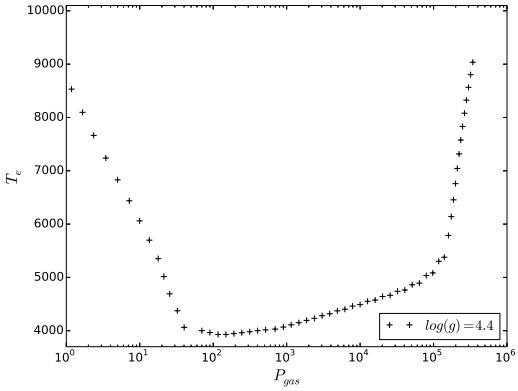

(b) Structure for the solar model. The maximum value of P_{gas} is 3.43×10^5 $dyn \cdot cm^{-2}$.

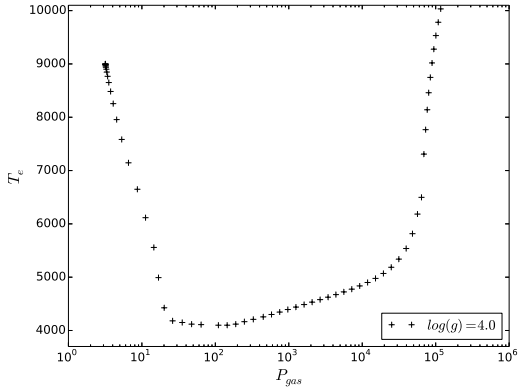

(c) Structure for the model with $\log(g) = 4.0$. The maximum value of P_{gas} is 1.17×10^5 $dyn \cdot cm^{-2}$.

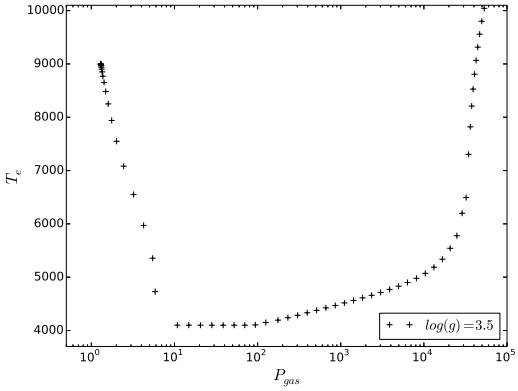

(d) Structure for the model with $\log(g) = 3.5$. The maximum value of P_{gas} is 5.31×10^4 $dyn \cdot cm^{-2}$.

Figure 5.2.: Structure of the best models for different gravity. Gas pressure is given in units of $dyn \cdot cm^{-2}$ and the temperature is the electron temperature in *Kelvins*. From left to right, the points correspond to the chromospheres towards the photosphere. All models have T_{eff} =5,800 K.

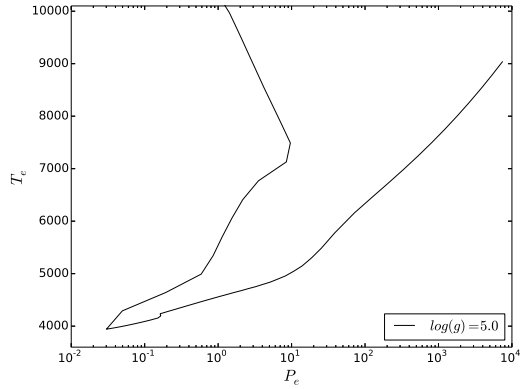

(a) Structure for the model with $\log(g) = 5.0$. The maximum value of P_{e^-} is 8.78×10^5 $dyn \cdot cm^{-2}$.

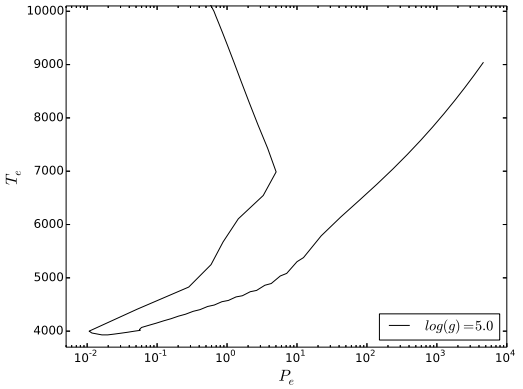

(b) Structure for the solar model. The maximum value of P_{e^-} is 3.43×10^5 $dyn \cdot cm^{-2}$.

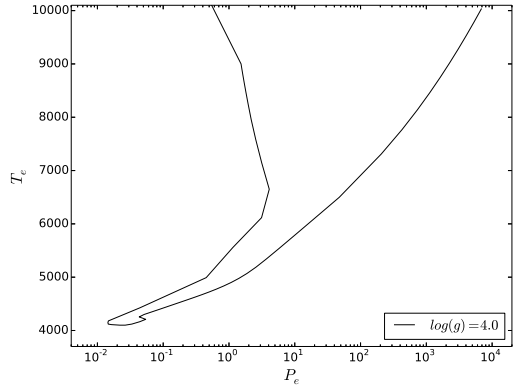

(c) Structure for the model with $\log(g) = 4.0$. The maximum value of P_{e^-} is 1.17×10^5 $dyn \cdot cm^{-2}$.

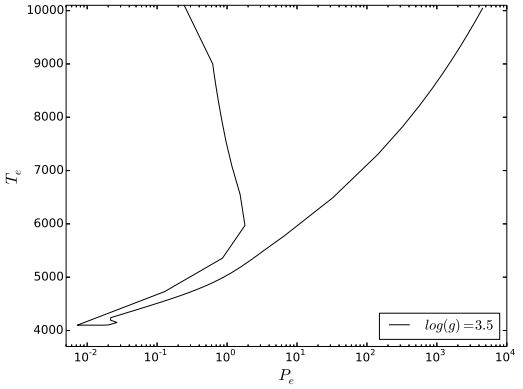

(d) Structure for the model with $\log(g) = 3.5$. The maximum value of P_{e^-} is 5.31×10^4 $dyn \cdot cm^{-2}$.

Figure 5.3.: Structure of the best models for different gravity. Gas pressure is given in units of $dyn \cdot cm^{-2}$ and the temperature is the electron temperature in *Kelvins*. From left to right, the points correspond to the chromospheres towards the photosphere. All models have T_{eff} =5,800 K.

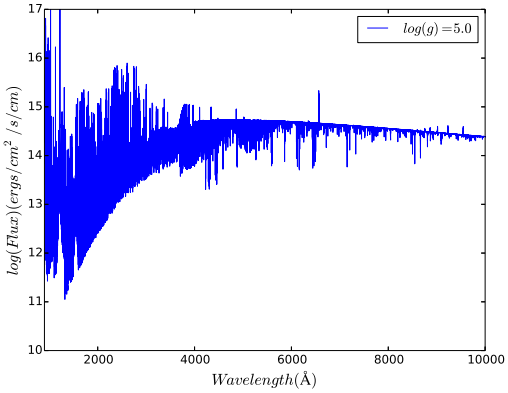

(a) SED for the model with $\log(g) = 5.0$.

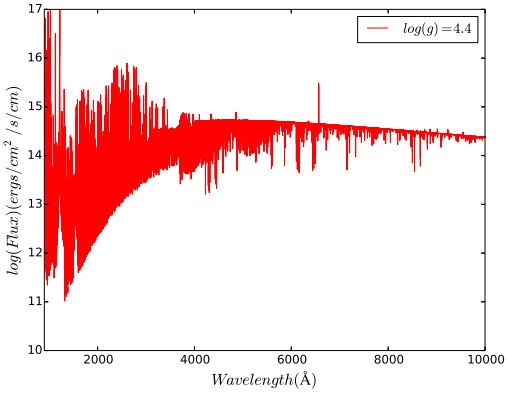

(b) SED for the solar model.

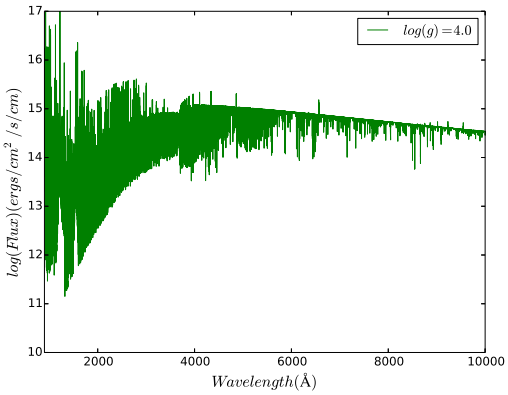

(c) SED for the model with $\log(g) = 4.0$.

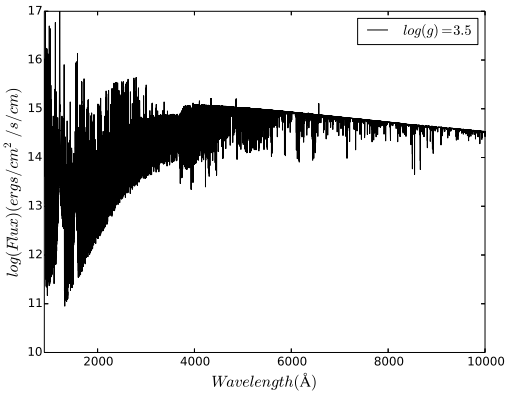

(d) SED for the model with $\log(g) = 3.5$.

Figure 5.4.: SED's of the best models with different surface gravity. All models have T_{eff} =5,800 K, $M = M_{\odot}$ and solar chemical composition. The presence of strong emission lines in the hydrogen continuum around 1,000 Å is due to LTE atomic lines in addition of the NLTE hydrogen lines.

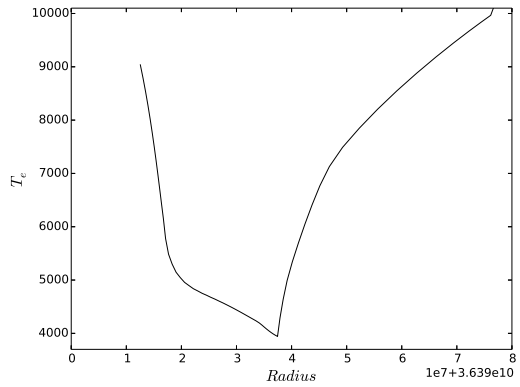

(a) Model with $\log(g) = 5.0$.

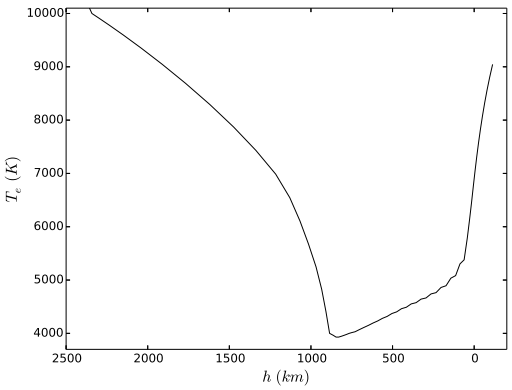

(b) Temperature profile for the solar model as a function of height.

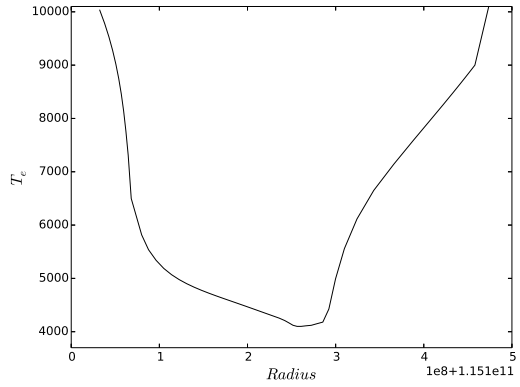

(c) Model with $\log(g) = 4.0$.

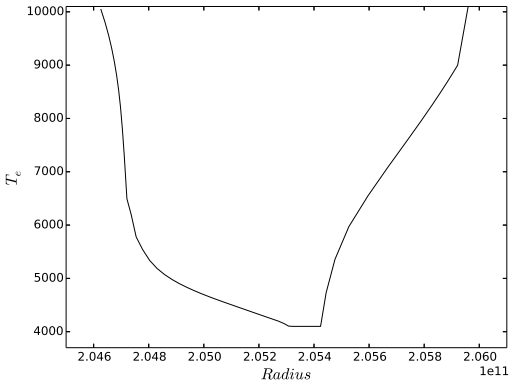

(d) Model with $\log(g) = 3.5$.

Figure 5.5.: Temperature profiles of the best models with different surface gravity. All models have T_{eff} =5,800 K, $M = M_{\odot}$ and solar chemical composition. Temperature is given in Kelvins and radii in *cm* except for the solar model, where the temperature is shown as a function of height. Height is given in kilometers measured above a zero point were $\tau_{5000} = 1$.

log(g)	W_0
5.0	0.35
4.4	0.43
4.0	0.51
3.5	0.55

Table 5.1.: Measured line widths of the Ca II K emission line for models of different surface gravities. The widths are given in Å.

One manner to do this was to plot of the lines in the same scale to compare them with each other and get the logarithm of the ratio of the widths. Once this was done, the difference in surface gravity were related in the following way:

$$\begin{aligned} &\log\left(W_a/W_b\right) = A \\ &\text{and} \\ &\log(g_a) - \log(g_b) = B \\ &\rightarrow W_{a,b} \propto g_{a,b}^{A/B} \end{aligned} \tag{5.1}$$

where a and b indicate two different modes, and $W_{a,b}$ is the ratio of the line widths of such models.

The second approach was to measure the line widths directly from each model: subtracting the minimums where the wings of the line begins to the maximum points and dividing by two gives us the values of flux whose wavelengths difference is the equivalent width. This was achieved with a small simple routine written in python but some ambiguities in the obtained values were observed. The main problem of this is that the region where a wing starts is not a well define point, but rather a group a points with very similar fluxes, making hard to select a single value to be the real minimum point.

5.3. Solar model

Testing models always requires the comparison with observational data. If both match, then one can trust the model even more. In this work, the K line for the solar model is to be compared with observations of a moderately active Sun in in 2014 (S=0.17) made with the TIGRE (*Telescopio Internacional de Guanajuato Robótico-Espectrocópico*, formerly *Hamburg Robotic Telescope*) and its HEROS (*Heidelberg Extended Range Optical Spectrograph.*) spectrograph (R=20,000 resolution).

But since all spectral lines, including photospheric absorption lines and chromospheric emission lines, are subjected to an extra broadening (besides pressure broadening) caused by the instruments, any model has to be convoluted with the Gaussian instrumental profile (IP) of the spectrograph that was used to get the observational data. Doppler broadening also affects the line widths, but the solar velocities of around $\sim 2\ km/s$ are not significative enough to be taken into account here.

The Gaussian function is describe as

$$G(x) = \frac{1}{\sigma\sqrt{2\pi}} \times e^{-(x-\mu)^2/(2\sigma^2)} \tag{5.2}$$

where σ is the standard deviation and μ is the mean. The TIGRE's spectrograph produces a broadening of about 0.2 Å, which is represented as $G(\lambda) = e^{-(\lambda-b)^2/c^2}a$, where $b = 3934.78$ Å is the center of the K line core, $c = 0.15$ Å is half the total width of the function, and $a = 1/c\sqrt{(2\pi)}$ is its total height.

Figure 5.6 illustrates the original solar model in the K line region (5.6(a)), the observational data (5.6(b)) of the solar Ca II K line core at its basal flux level in 2009 (S=0.15, Schröder et al. (2012)) and at an only moderately active level in 2014 (S=0.17) taken with the TIGRE, and the final convoluted synthetic spectra of this line with a Gaussian function for the TIGRE's HEROS spectrograph (5.6(c)) along with the 2014 data.

In the latter, it can be seen that the solar model includes as much emission as the basal flux shown by the Sun. Although the model still presents a stronger absorption core, this could only mean that the top of the chromosphere has a little too much column mass. But the temperature minimum is not affected by it because, as established before, the emission is produced at the bottom of the chromosphere and the absorption line outside the emission is caused by photospheric effects. Hence, the deepness of the core is not relevant.

5.4. Conclusions

Using the PHOENIX code, I have computed models with solar effective temperature and different surface gravity in order to see, if these would reproduce the Wilson-Bappu effect. This version of PHOENIX includes a chromospheric mode in hydrostatic equilibrium, with the same essential physics as summarized above, and which therefore simply scales with surface gravity ($cm \propto g^{-1/2}, n \propto g^{1/2}$). However, a practical problem occurs since shallow basal flux emission is too smeared out at already $\log(g) = 3.5$ (see figure 4.6). Consequently, I needed to make the bottom of the chromosphere (just above the temperature minimum) a little warmer to mimic the emission of modestly active stars, which in fact represent the stars observed for the WBE. But the equilibrium conditions allow only for

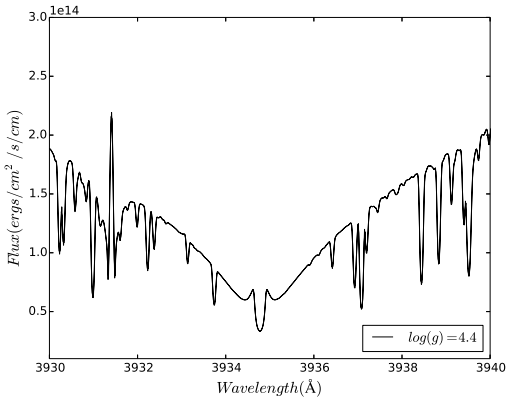

(a) Ca II K emission line of the PHOENIX solar model ($\log(g) = 4.4$).

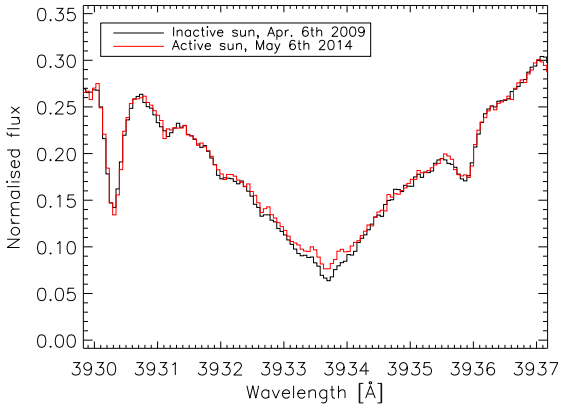

(b) Observational data of the solar Ca II K line core at its basal flux (black) and at a moderately active level (red).

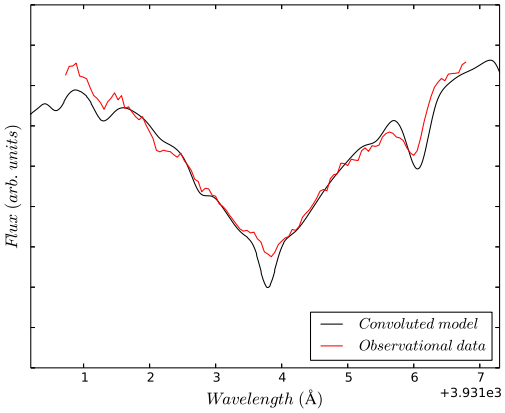

(c) Ca II K line core convoluted with a Gaussian instrumental profile of the TIGRE's spectrograph, and same observational data for the Sun at a moderately active level as in 5.6(b).

Figure 5.6.: Instrumental profile correction for the solar model in the Ca II K line region. The HEROS spectrograph of the TIGRE causes a broadening of about 0.2 Å, which levels the computed emission core of the solar model to the observational evidence.

a small margin on this.

I do not adjust any other parameter than surface gravity to obtain the emission line profiles, i.e., keeping turbulence velocities alike. Hence, these are produced from first principles and so represent a good test of the WBE explanation given by Ayres et al. (1975) nearly 40 years ago. As a result, the line widths reproduce the observed WBE gravity dependence with an exponent of -0.17 (rather than -0.25) very well and in absolute terms.

The employed method in this work for the computation of chromospheric models includes the approach of keeping mass, effective temperature, and metallicity the same for all models. The intention of the latter was to avoid unwanted effects in the line widths of the Ca II K emission line that may be produced by changes in such parameters. Even though this ensures us that increase of line widths are due to changes in gravity, the technique does not allow us to use a great range in values of surface gravity because effective temperatures become too large for smaller gravities.

This was the case of the models with $\log(g) = 2.5$ and $\log(g) = 2.0$, where no emission of the K line was observed but small modifications in the temperature profile and the column mass (trying to get emission peaks) were not possible because the models were too instable by themselves to be recomputed with new parameters. An alternative to make this work is to compute photospheric models more consistent with low gravity stars, adjusting T_{eff}, mass and radii, and to build the chromospheres from them, obtaining more stable full models.

In this work I present the first sample of chromospheric models to demonstrate the WBR over a range of surface gravity to date. The models show that for at least the range of surface gravity $3.5 \leq \log(g) \leq 5.0$ the WBR is linear and behaves like

$$W_0 \propto g^{-0.17\pm0.02} \tag{5.3}$$

Equation (5.3) seems to be well calibrated in comparison with previous studies (Wilson, 1967; Reimers, 1973; Pace et al., 2003; Park et al., 2013). It was obtained from the first three rows in table 5.2, which shows the different relations of the line widths with surface gravity when the models for $\log(g) = 5.0, 4.4$, and 4.0 are compared with each other. The error has been found statistically from the different measurements.

The following three rows correspond to the comparison made of the $\log(g) = 3.5$ model with the rest of them. As can been seen, the difference in the third column increases when this model is used. Actually, the power of g decreases for models with lower surface gravity and hence, gets far away from the previously reported value of -0.17 by Park et al. (2013). The main reason for this to happen and to not use this model to get the

relation (5.3), is that the models lose consistency as surface gravity gets lower because the rest of the parameters (effective temperature, turbulence velocity, mass, etc.) were not selected to match such values of gravity and hence, they are not very reliable.

Model a	**Model b**	**Power of g**
5.0	4.4	-0.15
5.0	4.0	-0.16
4.4	4.0	-0.18
3.5	5.0	-0.13
3.5	4.4	-0.12
3.5	4.0	-0.07

Table 5.2.: W_0 relation with gravity as measured from the models. Each row gives the power of g in the relation (5.3) when the listed **a** and **b** models are compared with each other.

It is observed that both the photosphere and chromosphere of the models are more extended in height by the same factor with decreasing gravity, as described by Avrett (1972). At the temperature minimum, τ also increases with decreasing gravity: for the $\log(g) = 3.5$ and $\log(g) = 5.0$ models, the first has a τ more than twice as the second one (2.158×10^{-3} and 1.098×10^{-3}, respectively). This increased thickness leads to a greater width of the line because it originates above T_{min}. For greater thickness, the photosphere can be seen farther out in the wings of a line, like explained in figure A.1.

In the solar case, which is used as a first test, the minimum temperature is found (over height, single component) for a relatively inactive Sun to reach down to 3,930 K. The respective PHOENIX model ($\log(g) = 4.4$) matches width and typical flux of the chromospheric Ca II emission of a nearly inactive Sun, as observed with the Hamburg robotic telescope (see figure5.6(b)). For comparison, the quiet Sun model of Vernazza et al. (1973) had a temperature minimum of 4,170 K (figure 1.3).

5.5. Future work

As mentioned in 5.4, the models with gravities lower than $\log(g) = 3.5$ did not present any emission of the Ca II K line. To continue this work and extend the W_0 relation with gravity to a greater range of gravities, more consistent photospheric models for low gravity stars are needed.

First of all, to compute good photospheric models, the adequate stellar parameters must be selected to (1) construct well behaved atmospheres and (2) to match the respective

chromospheres that are to be constructed above them and which must present sufficient emission of the Ca II K line to be measured.

The above will allow not only to measure K line widths, but to measure K line widths that are consistent with low gravity stars and all of the parameter that determine their photospheric and chromospheric structure. Hence, the results of the corresponding WBE in terms of surface gravity will be even more accurate and reliable than the one presented here.

Furthermore and to keep testing the reproducibility of the WBE, the line widths of the Mg II k emission line of the same models will be also measured to see how do they behave with changing gravity. As mentioned before (see §2.2), the k line is also expected to quantitatively follow the WBE, although in a smaller degree than the K line.

Finally, as the solar model in the present work was compared with observational data, the solar k line will also be adjusted to compare with solar observations in the UV regime by moonlight[1].

[1]This data is already available.

A

Equations for the method

A.1. Radiative transfer equation

Radiant energy conservation can be mathematically described by the equation of radiative transfer. Its derivation for atmospheres adopting a plane parallel configuration[1], like PHOENIX does, can begin with the assumption of traveling radiation of intensity $I_\nu(r, \theta, t)$.

Let us suppose this radiation goes through the length dr and cross section $d\sigma$ in the time dt but only in the frequency interval $d\nu$. If the direction of the intensity θ is normal to $d\sigma$ and passes by a solid angle $d\omega$, then the emergent intensity will be different by an amount of energy which is the absorbed and emitted energy within the volume element previously describe. Therefore,

$$[I_\nu(r + \Delta r, \theta, t + \Delta t) - I_\nu(r, \theta, t)]d\sigma d\omega d\nu dt = [j_\nu(r, \theta, t) - \kappa_\nu(r, \theta, t)I_\nu(r, \theta, t)]ds d\sigma d\omega d\nu dt \tag{A.1}$$

j_ν and κ_ν are the emission and absorption coefficients, respectively. Now let s be the length traveled by the ray, so $\Delta t = \Delta s/c$, c being the speed of light, and we get

$$I_\nu(r + \Delta r, \theta, t + \Delta t) - I_\nu(r, \theta, t) = \left(\frac{1}{c}\frac{\partial I_\nu}{\partial t} + \frac{\partial I_\nu}{\partial s}\right) ds \tag{A.2}$$

For time independent transfer equation and combining equations (A.1) and (A.2):

$$j_\nu - \kappa_\nu I_\nu = \frac{\partial I_\nu}{\partial s} \tag{A.3}$$

[1] Approximation in which all parameters depend on one direction.

When the geometry of the medium is divided into plane parallel layers and the angle between the ray with its normal $\hat{z}$ is $\theta = cos^{-1}\mu$ we finally can write (A.3) as

$$j_\nu - \kappa_\nu I_\nu = \mu \frac{\partial I_\nu}{\partial z} \tag{A.4}$$

Equation (A.4) is the RTE for plane parallel atmospheres.

A.2. Source function

The line source function (S_ν) is defined as the ratio of monochromatic emission coefficient to monochromatic absorption coefficient due to line processes but it may also be written as

$$S_\nu = (1 - \epsilon) \int_0^\infty \varphi_\nu J_\nu d\nu + \epsilon B_\nu(T) \tag{A.5}$$

where ϵ is the destruction probability, φ_ν is the line profile function, J_ν is the mean specific intensity and $B_\nu(T)$ is the Planck function.

The destruction probability (ϵ) tells us wether photons are destroyed by thermal processes or isotropically scattered without changing their frequency. This is reflected in different layers of an atmosphere: for deep layers (towards the core), the thermal term in equation (A.5) dominates because collisions are important. In that case LTE is valid and $S_\nu = B_\nu(T)$. On the other hand, when moving outwards through the atmosphere, scattering is dominant because of the extended chromospheres lead to a larger mean free path, until at some point we reach the region where photons are being lost from the star.

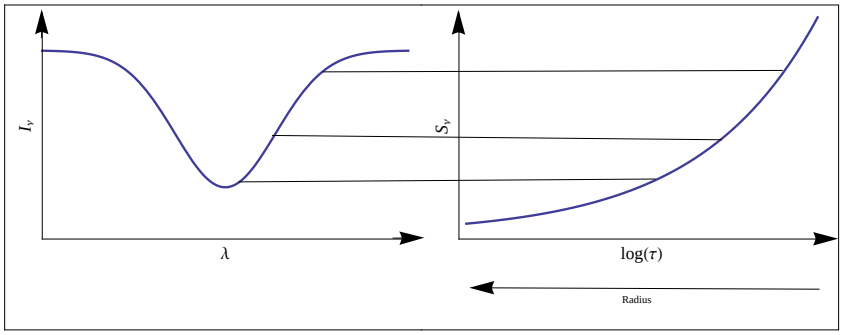

Figure A.1.: The figure shows the relation between the increase of the source function with different zones of an absorption line and the radius of the atmosphere.

This means the source function decreases outwards because temperatures drop and so the Planck function (and hence J_ν because in this region $S_\nu = J_\nu$), and optical depths get smaller as well. Therefore, we get an absorption line from the outer layers of the atmosphere while its wings are being formed in deeper layers than the line core; this is illustrated in figure A.1.

A.3. Saha equation

To describe systems like molecules, atoms or electrons, it is essential to know the energies of their quantum states. For a large number of particles, it is also necessary to include the way they distribute themselves throughout the allowed anergy levels.

The well-known Maxwell-Boltzmann statistics equation (A.6) is useful to count the number of atoms in a particular energy level and the abundances of different types of atoms, for different excitation states but only in one particular ionization state. It gives the fraction of atoms of a given sort (elements) which are in a certain level, in its simplest form, it provides a ratio of the number of atoms in two particular levels.

$$\frac{N^i}{N_1^i} = \frac{1}{g_1^i} \sum_{j=1}^{\infty} g_j^i e^{-\frac{E_j^i - E_1^i}{\kappa T}} \tag{A.6}$$

where N^i is the number of ions in ionization state i, N_1^i is the number of ions in the ground state of ionization state i, g_1^i is the statistical weight of the ground state of ionization state i, g_j^i are the statistical weights of excited states j of ionization state i, E_1^i is the energy of the ground state of ionization state i, E_j^i are the energies of excites states j of ionization state i, and κ is the Boltzmann's constant.

To do the same for a following ionization state, let us say the state $i+1$, one has to take into account not only the excitation states of the ion $i+1$, but also of the free electrons, whose energies and statistical weights are determined by $E_e = P_e^2/2m_e$ and $g_e(P_e) = \frac{2}{h^3}\frac{1}{n_e} 4\pi P_e^2$, respectively; P_e is the momentum, m_e is the electron mass, n_e is the number density of free electrons, and h is the Planck's constant. This leads to

$$\frac{N^i + 1}{N_1^i} = \frac{Z^{i+1}}{Zi} \frac{2}{n_e h^3} \left(2\pi m_e \kappa T\right)^{3/2} e^{-\chi_i/\kappa T} \tag{A.7}$$

with $Z^i := \sum_{j=1}^{\infty} g_j^i e^{-\frac{E_j^i - E_1^i}{\kappa T}}$. Equation (A.7) is called the *Saha equation*, which gives the relative number of atoms of a given species that are in two ionization states in thermal

equilibrium as a function of electron density and temperature.

B

Temperature profiles

B.1. Corrections to chromospheres

The corrected temperature profiles for solar models are listed below. They include temperature T in $Kelvins$, radius R in $centimeters$ and column mass cm in gr/cm^2 values. Each one of them consists in 64 points corresponding to the layers that constitute the photospheres.

	$\mathbf{T}(10^3)$ **(K)**		$\mathbf{R}(10^{10})$ **(cm)**	**cm** (gr/cm^2)
1	2	3		
20.000	20.000	20.000	7.3064	1.7268e-06
1.0000	10.000	10.000	7.2965	1.7268e-05
9.7061	9.7061	9.7061	7.2951	2.2104e-05
9.3531	9.3531	9.3531	7.2935	2.9739e-05
8.9560	8.9560	8.9560	7.2916	4.1522e-05
8.5321	8.5321	8.5321	7.2897	5.9293e-05
8.0971	8.0971	8.0971	7.2878	8.5458e-05
7.6634	7.6634	7.6634	7.2859	1.2304e-04
7.2393	7.2393	7.2393	7.2842	1.7572e-04
6.8297	6.8297	6.8297	7.2827	2.4793e-04
6.4366	6.4366	6.4366	7.2813	3.4500e-04
6.0600	6.0600	6.0600	7.2803	4.7343e-04
5.6989	5.6989	5.6989	7.2796	6.4130e-04
5.3515	5.3515	5.3515	7.2791	8.5873e-04
5.0159	5.0159	5.0159	7.2787	1.1385e-03
4.6904	4.6904	4.6904	7.2784	1.4967e-03
4.3732	4.3732	4.3732	7.2781	1.9539e-03
4.0627	4.0627	4.0627	7.2779	2.5366e-03

Continued on next page...

	$\mathbf{T}(10^3)$ **(K)**		$\mathbf{R}(10^{10})$ **(cm)**	**cm** (gr/cm^2)
1	2	3		
4.0000	4.0000	4.0000	7.2777	3.2788e-03
4.0000	3.9650	3.9650	7.2775	4.2243e-03
4.0000	3.9300	3.9300	7.2774	5.4295e-03
4.0000	3.8950	3.9300	7.2772	6.9662e-03
4.0000	3.8600	3.9450	7.2770	8.9261e-03
4.0000	3.8950	3.9620	7.2769	1.1426e-02
4.0000	3.9300	3.9800	7.2767	1.4614e-02
4.0000	3.9650	4.0000	7.2766	1.8679e-02
4.0000	4.0000	4.0150	7.2764	2.3861e-02
4.0301	4.0301	4.0301	7.2762	3.0463e-02
4.0690	4.0690	4.0690	7.2759	3.8868e-02
4.1099	4.1099	4.1099	7.2757	4.9563e-02
4.1496	4.1496	4.1496	7.2754	6.3160e-02
4.1938	4.1938	4.1938	7.2751	8.0427e-02
4.2327	4.2327	4.2327	7.2748	1.0234e-01
4.2814	4.2814	4.2814	7.2745	1.3010e-01
4.3177	4.3177	4.3177	7.2742	1.6529e-01
4.3717	4.3717	4.3717	7.2739	2.0976e-01
4.4033	4.4033	4.4033	7.2736	2.6604e-01
4.4627	4.4627	4.4627	7.2733	3.3700e-01
4.4899	4.4899	4.4899	7.2730	4.2675e-01
4.5524	4.5524	4.5524	7.2727	5.3975e-01
4.5758	4.5758	4.5758	7.2724	6.8268e-01
4.6421	4.6421	4.6421	7.2721	8.6236e-01
4.6641	4.6641	4.6641	7.2718	1.0895e+00
4.7396	4.7396	4.7396	7.2715	1.3736e+00
4.7636	4.7636	4.7636	7.2712	1.7314e+00
4.8609	4.8609	4.8609	7.2709	2.1722e+00
4.8930	4.8930	4.8930	7.2706	2.7195e+00
5.0349	5.0349	5.0349	7.2703	3.3664e+00
5.0831	5.0831	5.0831	7.2700	4.1411e+00
5.3029	5.3029	5.3029	7.2698	4.9755e+00
5.3789	5.3789	5.3789	7.2695	5.9031e+00
5.7875	5.7875	5.7875	7.2693	6.6896e+00
6.1403	6.1403	6.1403	7.2692	7.2867e+00
6.4542	6.4542	6.4542	7.2690	7.8015e+00
6.7583	6.7583	6.7583	7.2689	8.2798e+00
7.0439	7.0439	7.0439	7.2688	8.7490e+00
7.3151	7.3151	7.3151	7.2687	9.2304e+00

Continued on next page...

	$\mathbf{T}(10^3)$ **(K)**		$\mathbf{R}(10^{10})$ **(cm)**	**cm** (gr/cm^2)
1	2	3		
7.5765	7.5765	7.5765	7.2686	9.7399e+00
7.8310	7.8310	7.8310	7.2685	1.0290e+01
8.0801	8.0801	8.0801	7.2684	1.0894e+01
8.3247	8.3247	8.3247	7.2682	1.1564e+01
8.5653	8.5653	8.5653	7.2681	1.2314e+01
8.8024	8.8024	8.8024	7.2679	1.3161e+01
9.0364	9.0364	9.0364	7.2678	1.4124e+01

Table B.1.: Modified temperature profiles for solar chromosphere models.

B.2. Models with different gravities

The final output temperature profiles for models of different gravities are listed below. They only include temperature T in $Kelvins$ and radius R in $centimeters$. Each one of them consists in 64 points corresponding to the layers that constitute the photospheres and chromospheres. Columns are numbered according to the value of $\log(g)$.

		$\mathbf{T}(10^3)$ **(K)**		**R (cm)**			
5.0	4.4	4.0	3.5	$5.0(10^{10})$	$4.4(10^{10})$	$4.0(10^{11})$	$3.5(10^{11})$
20.000	19.931	19.999	19.999	7.3064	3.6501	1.1571	2.0630
1.0000	9.9655	9.0000	9.0000	7.2965	3.6466	1.1555	2.0592
9.7061	9.8405	8.9983	8.9983	7.2951	3.6464	1.1555	2.0592
9.3531	9.6686	8.9957	8.9958	7.2935	3.6462	1.1555	2.0592
8.9560	9.4477	8.9917	8.9919	7.2916	3.6459	1.1555	2.0592
8.5321	9.1816	8.9855	8.9858	7.2897	3.6456	1.1555	2.0591
8.0971	8.8790	8.9758	8.9762	7.2878	3.6452	1.1555	2.0591
7.6634	8.5500	8.9608	8.9614	7.2859	3.6449	1.1555	2.0591
7.2393	8.2041	8.9377	8.9386	7.2842	3.6445	1.1555	2.0591
6.8297	7.8489	8.9022	8.9035	7.2827	3.6442	1.1555	2.0591
6.4366	7.4894	8.8485	8.8501	7.2813	3.6439	1.1555	2.0590
6.0600	7.1285	8.7681	8.7700	7.2803	3.6436	1.1554	2.0589
5.6989	6.7682	8.6506	8.6520	7.2796	3.6435	1.1554	2.0587
5.3515	6.4093	8.4835	8.4830	7.2791	3.6433	1.1553	2.0585
5.0159	6.0521	8.2548	8.2492	7.2787	3.6432	1.1552	2.0582
4.6904	5.6967	7.9556	7.9396	7.2784	3.6431	1.1550	2.0578
4.3732	5.3431	7.5836	7.5496	7.2781	3.6430	1.1548	2.0573

Continued on next page...

T(10^3) (K)				R (cm)			
5.0	4.4	4.0	3.5	5.0(10^{10})	4.4(10^{10})	4.0(10^{11})	3.5(10^{11})
4.0627	4.9911	7.1443	7.0829	7.2779	3.6429	1.1546	2.0566
4.0000	4.6406	6.6496	6.5516	7.2777	3.6428	1.1544	2.0559
3.9650	4.2911	6.1154	5.9708	7.2775	3.6427	1.1542	2.0552
3.9300	3.9425	5.5580	5.3569	7.2774	3.6427	1.1540	2.0547
3.9300	3.9646	4.9914	4.7291	7.2772	3.6427	1.1539	2.0544
3.9450	3.9897	4.4247	4.1000	7.2770	3.6426	1.1539	2.0542
3.9620	4.0178	4.1800	4.1000	7.2769	3.6426	1.1538	2.0540
3.9800	4.0487	4.1500	4.1000	7.2767	3.6425	1.1537	2.0538
4.0000	4.0821	4.1200	4.1000	7.2766	3.6425	1.1537	2.0537
4.0150	4.1177	4.1100	4.1000	7.2764	3.6425	1.1536	2.0535
4.0301	4.1553	4.1000	4.1000	7.2762	3.6424	1.1536	2.0533
4.0690	4.1947	4.1000	4.1000	7.2759	3.6424	1.1535	2.0532
4.1099	4.2355	4.1204	4.1041	7.2757	3.6423	1.1535	2.0530
4.1496	4.2774	4.1648	4.1497	7.2754	3.6422	1.1534	2.0529
4.1938	4.3199	4.2094	4.1949	7.2751	3.6422	1.1534	2.0527
4.2327	4.3626	4.2545	4.2403	7.2748	3.6421	1.1533	2.0524
4.2814	4.4049	4.3003	4.2859	7.2745	3.6420	1.1532	2.0522
4.3177	4.4466	4.3465	4.3316	7.2742	3.6419	1.1532	2.0519
4.3717	4.4874	4.3931	4.3776	7.2739	3.6419	1.1531	2.0517
4.4033	4.5270	4.4398	4.4237	7.2736	3.6418	1.1530	2.0514
4.4627	4.5661	4.4863	4.4697	7.2733	3.6417	1.1529	2.0511
4.4899	4.6032	4.5325	4.5159	7.2730	3.6416	1.1528	2.0509
4.5524	4.6414	4.5786	4.5626	7.2727	3.6416	1.1528	2.0506
4.5758	4.6765	4.6252	4.6107	7.2724	3.6415	1.1527	2.0504
4.6421	4.7156	4.6729	4.6608	7.2721	3.6414	1.1526	2.0501
4.6641	4.7512	4.7228	4.7139	7.2718	3.6413	1.1525	2.0499
4.7396	4.7954	4.7763	4.7707	7.2715	3.6412	1.1524	2.0496
4.7636	4.8373	4.8348	4.8324	7.2712	3.6412	1.1523	2.0493
4.8609	4.8957	4.9005	4.9006	7.2709	3.6411	1.1523	2.0491
4.8930	4.9558	4.9773	4.9794	7.2706	3.6410	1.1522	2.0488
5.0349	5.0457	5.0699	5.0718	7.2703	3.6409	1.1521	2.0485
5.0831	5.1464	5.1865	5.1869	7.2700	3.6409	1.1520	2.0483
5.3029	5.3000	5.3396	5.3376	7.2698	3.6408	1.1519	2.0480
5.3789	5.4851	5.5376	5.5426	7.2695	3.6407	1.1518	2.0477
5.7875	5.7769	5.8155	5.7777	7.2693	3.6407	1.1517	2.0475
6.1403	6.1574	6.1845	6.1994	7.2692	3.6406	1.1517	2.0473
6.4542	6.4406	6.4979	6.4935	7.2690	3.6406	1.1516	2.0472
6.7583	6.7148	7.3096	7.3039	7.2689	3.6406	1.1516	2.0471
7.0439	6.9807	7.7665	7.8186	7.2688	3.6405	1.1516	2.0470

Continued on next page...

T(10^3) (K)				**R (cm)**			
5.0	4.4	4.0	3.5	5.0(10^{10})	4.4(10^{10})	4.0(10^{11})	3.5(10^{11})
7.3151	7.2415	8.1396	8.2104	7.2687	3.6405	1.1515	2.0469
7.5765	7.5002	8.4590	8.5279	7.2686	3.6405	1.1515	2.0469
7.8310	7.7580	8.7475	8.8072	7.2685	3.6404	1.1515	2.0468
8.0801	8.0156	9.0180	9.0666	7.2684	3.6404	1.1515	2.0467
8.3247	8.2727	9.2779	9.3154	7.2682	3.6403	1.1514	2.0466
8.5653	8.5289	9.5317	9.5590	7.2681	3.6403	1.1514	2.0465
8.8024	8.7837	9.7822	9.8010	7.2679	3.6403	1.1513	2.0464
9.0364	9.0370	1.0031	1.0043	7.2678	3.6402	1.1513	2.0462

Table B.2.: Temperature profiles of the models with different gravities.

References

Allard, F. and Hauschildt, P.: 1995, *ApJ* **445**, 433

Avrett, E.: 1972, *NASA SP* **317**, 27

Avrett, E. and Linsky, J.: 1970, *BAAS* **2**, 181

Ayres, T.: 1979, *ApJ* **228**, 509

Ayres, T., Linsky, J., and Shine, R.: 1975, *ApJ* **195**, 121

Baliunas, S., Donahue, R., Soon, W., Horne, J., Frazer, J., and Woodard-Eklund, L.: 1995, *ApJ* **438**, 269

Baron, E., Hauschildt, P., and Allard, F.: 2003, *IAUS* **210**, 19

Dupree, A. and Smith, G.: 1995, *ApJ* **110**, 405

Fuhrmeister, B., Schmitt, J., and Hauschildt, P.: 2005, *A&A* **439**, 1137

Gingerich, O., Noyes, R., Kalkofen, W., and Cuny, Y.: 1971, *Solar Physics* **18**, 347

Gómez, T.: 2012, *PASP* **124**, 1246

Hauschildt, P., Allard, F., Alexander, D., Schweitzer, A., and Baron, E.: 1996, *IAUS* **176**, 539

Hauschildt, P. and Baron, E.: 1999, *CoAM* **109**, 41

Houdebine, E., Doyle, J., and Kościelecki: 1995, *A&A* **294**, 773

Hubeny, I.: 2003, *ASP Conference Series* **288**, 17

Jevremovic, D., Doyle, J., and Short, C.: 2000, *A&A* **358**, 575

Kondo, Y., Giuli, R., Modisette, J., and Rydgren, A.: 1972, *ApJ* **176**, 153

Kraft, R., Preston, G., and Wolff, S.: 1964, *ApJ* **140**, 235

Kurucz, R. and Bell, B.: 1995, *Smithsonian Astrophysics Observatory* **48**, CDROM23

Linsky, J. and Avrett, E.: 1970, *PASP* **82**, 169

Linsky, J. and Haisch, B.: 1979, *ApJ* **229**, 27

Maltby, P., Avrett, E., Carlsson, M., Kjeldseth, O., Kurucz, R., and Loeser, R.: 1986, *ApJ* **306**, 284

Narain, U. and Ulmschneider, P.: 1990, *SSRv* **54**, 377

Neckel, H.: 1974, *A&A* **35**, 99

Olson, G. and Kunasz, P.: 1987, *JQSRT* **38**, 325

Pace, G., Pasquini, L., and Ortolani, S.: 2003, *A&A* **401**, 997

Park, S., Kang, W., Lee, J., and Lee, S.: 2013, *AJ* **146**, 73

Reimers, D.: 1973, *A&A* **24**, 79

Rothman, R., Gamache, R., and Tipping, C.: 1992, *JQSRT* **48**, 469

Schröder, K.-P., Mittag, M., Pérez-Martínez, M., and Cuntz, M.: 2012, *A&A* **540**, A130

Ulmschneider, P.: 2003, *ASPC* **286**, 363

Vaughan, A., Preston, W., and Wilson, O.: 1978, *PASP* **90**, 267

Vernazza, J., Avrett, E., and Loeser, R.: 1973, *ApJ* **184**, 605

Wallerstein, G., Machado-Pelaez, L., and González, G.: 1999, *PASP* **111**, 335

Wilson, O.: 1967, *PASP* **79**, 46

Wilson, O.: 1978, *ApJ* **226**, 379

Wilson, O. and Bappu, M.: 1957, *ApJ* **125**, 661

Zirin, H.: 1971, *Phil. Trans. Roy. Soc. London* **A270**, 183